(12) **United States Patent**
Verduzco et al.

(10) **Patent No.:** **US 11,739,010 B2**
(45) **Date of Patent:** **Aug. 29, 2023**

(54) **ELECTRODES FOR SELECTIVE REMOVAL OF MULTIVALENT IONS THROUGH CAPACITIVE DEIONIZATION**

(71) Applicant: **William Marsh Rice University**, Houston, TX (US)

(72) Inventors: **Rafael Verduzco**, Houston, TX (US); **Amit Jain**, Houston, TX (US); **Jun Kim**, Houston, TX (US); **Qilin Li**, Houston, TX (US); **Kuichang Zuo**, Houston, TX (US)

(73) Assignee: **William Marsh Rice University**, Houston, TX (US)

(*) Notice: Subject to any disclaimer, the term of this patent is extended or adjusted under 35 U.S.C. 154(b) by 967 days.

(21) Appl. No.: **16/533,402**

(22) Filed: **Aug. 6, 2019**

(65) **Prior Publication Data**

US 2020/0071200 A1 Mar. 5, 2020

Related U.S. Application Data

(60) Provisional application No. 62/715,116, filed on Aug. 6, 2018.

(51) **Int. Cl.**
C02F 1/469	(2023.01)
B01D 15/36	(2006.01)
C02F 1/461	(2023.01)

(52) **U.S. Cl.**
CPC *C02F 1/4691* (2013.01); *B01D 15/362* (2013.01); *B01D 15/363* (2013.01); *C02F 1/46114* (2013.01)

(58) **Field of Classification Search**
CPC C02F 1/4691; B01D 15/362
See application file for complete search history.

(56) **References Cited**

U.S. PATENT DOCUMENTS

9,771,282 B2 *	9/2017	Cho	....	C02F 1/4691
10,376,874 B2 *	8/2019	Choi	....	C08F 20/58
10,626,028 B2 *	4/2020	Mayes	....	C02F 1/4691
2016/0272515 A1 *	9/2016	Choi	....	C25B 11/04

* cited by examiner

Primary Examiner — Sikarl A Witherspoon
(74) *Attorney, Agent, or Firm* — Osha Bergman Watanabe & Burton LLP

(57) **ABSTRACT**

A method of forming an electrode for capacitive deionization includes depositing an slurry onto a substrate, wherein the slurry comprises a porous material, a first crosslinkable hydrophilic polymer, and a crosslinker for the first crosslinkable hydrophilic polymer; annealing the slurry deposited on the substrate to create a crosslinked porous layer on the substrate; depositing an solution comprising an ion-exchange material, a second crosslinkable hydrophilic polymer, and a crosslinker for the second crosslinkable hydrophilic polymer onto the crosslinked porous layer; and optionally annealing and/or drying the solution on the crosslinked porous layer.

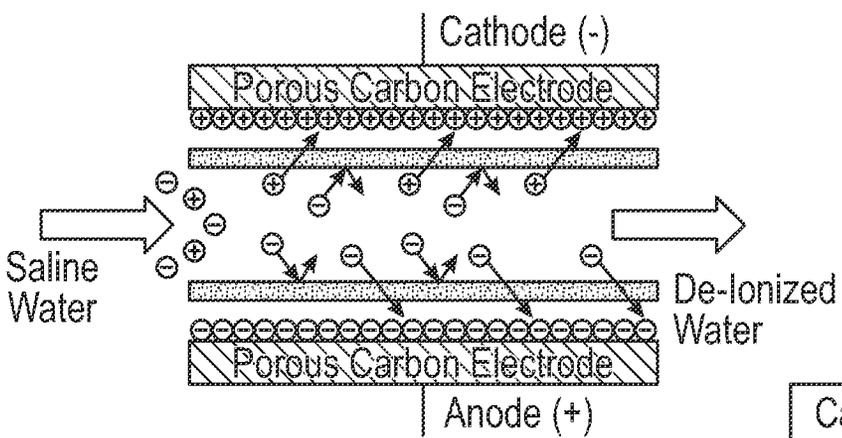**17 Claims, 25 Drawing Sheets**

Cathode (-)

Porous Carbon Electrode

Saline
Water

De-Ionized
Water

Porous Carbon Electrode

Anode (+)

| Cation | $\oplus$ |
| Anion | $\ominus$ |

FIG. 1A
(Prior Art)

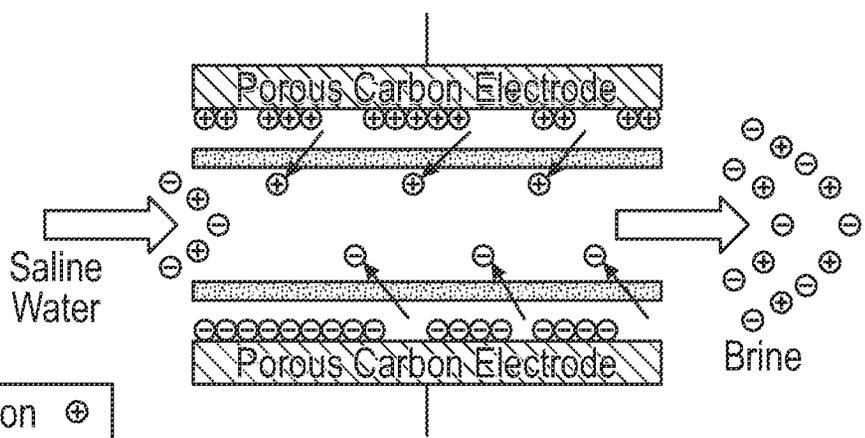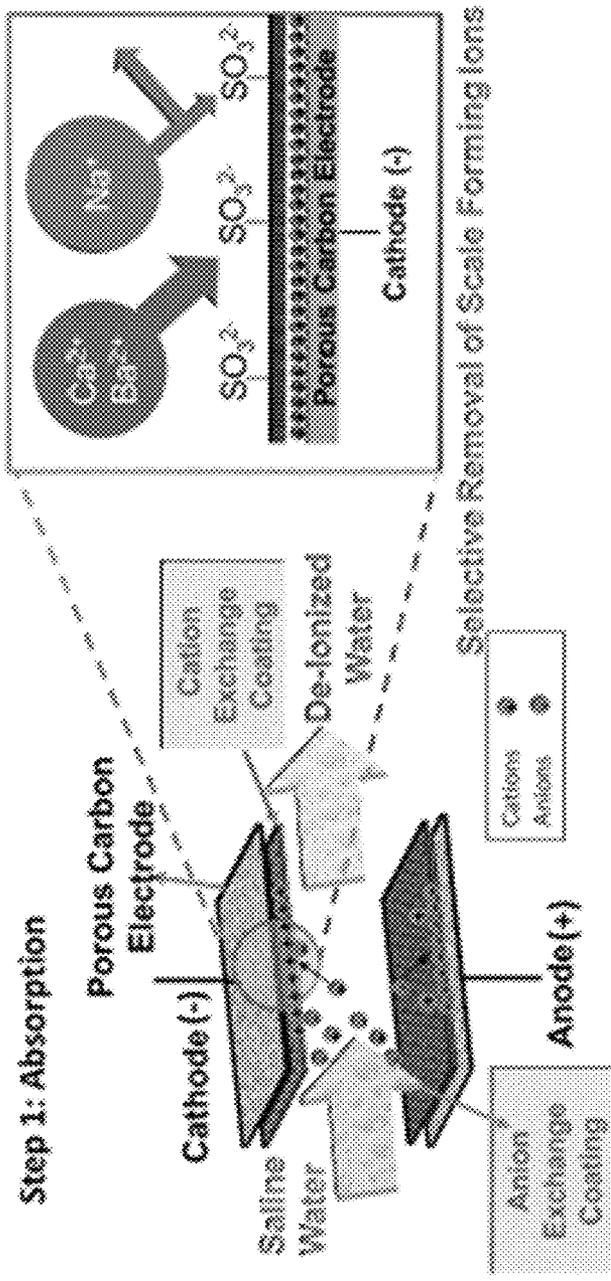Porous Carbon Electrode

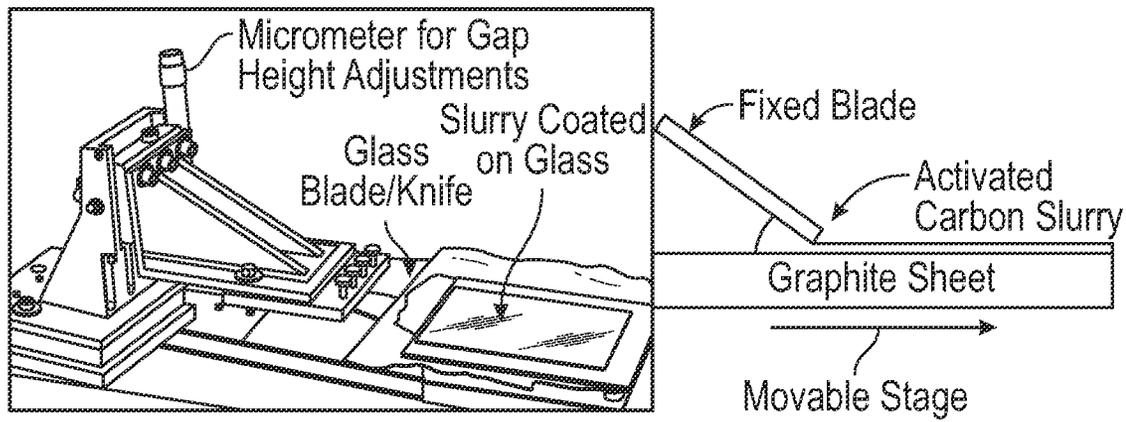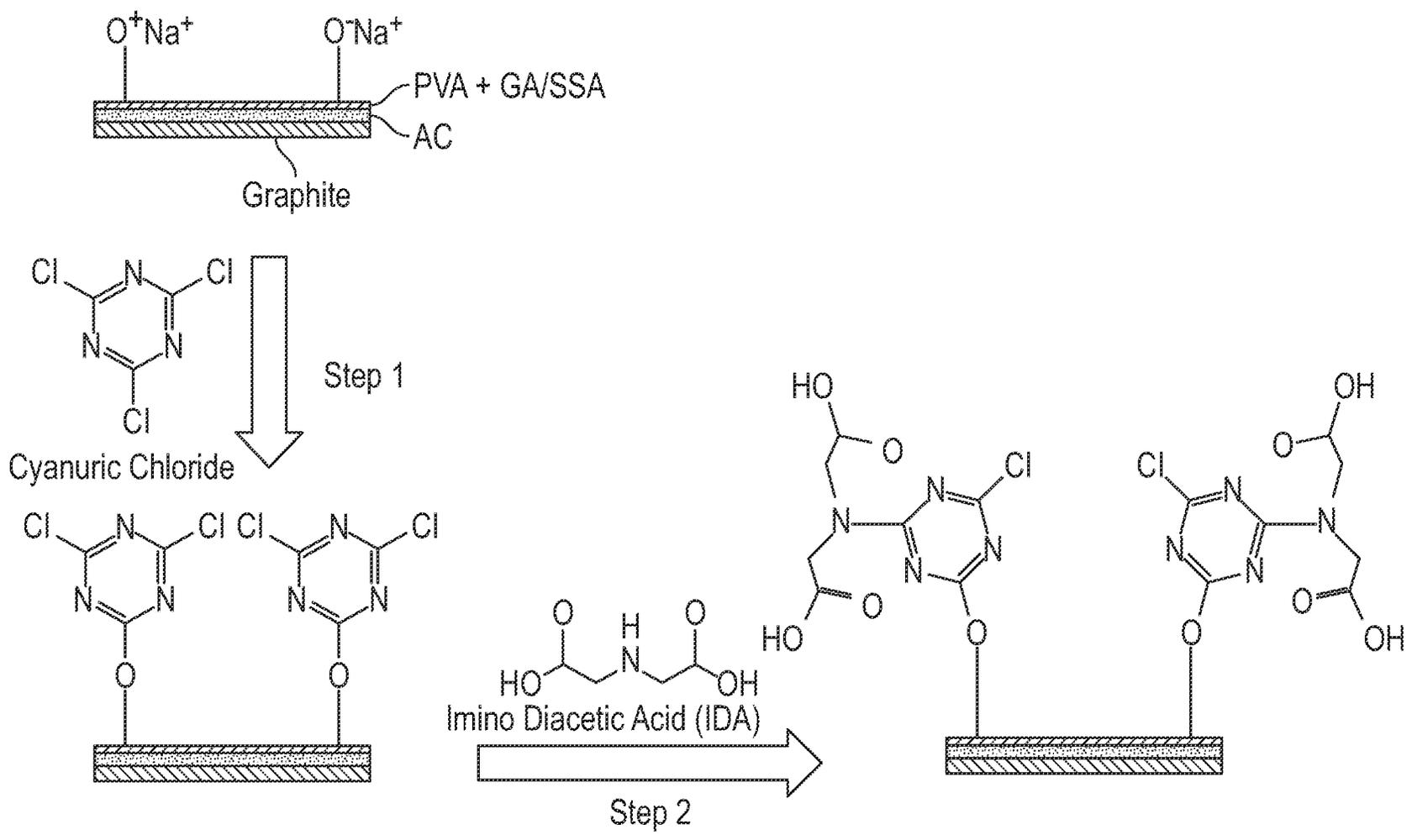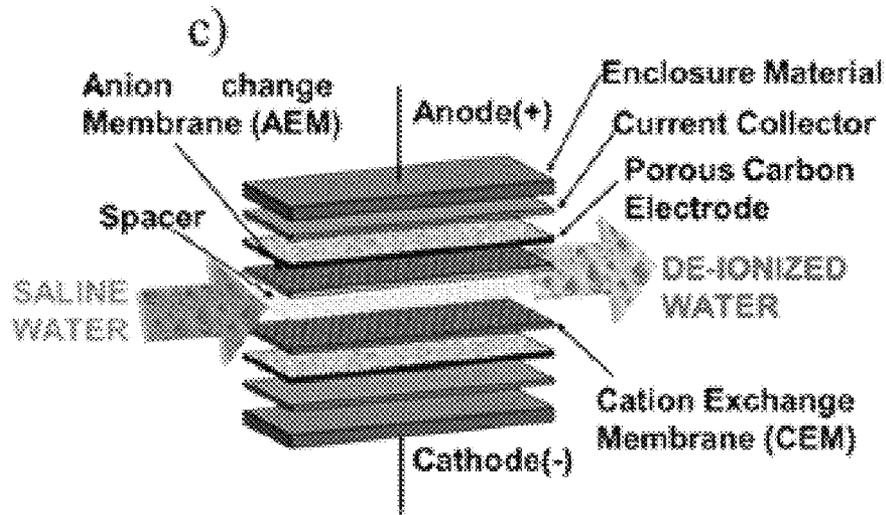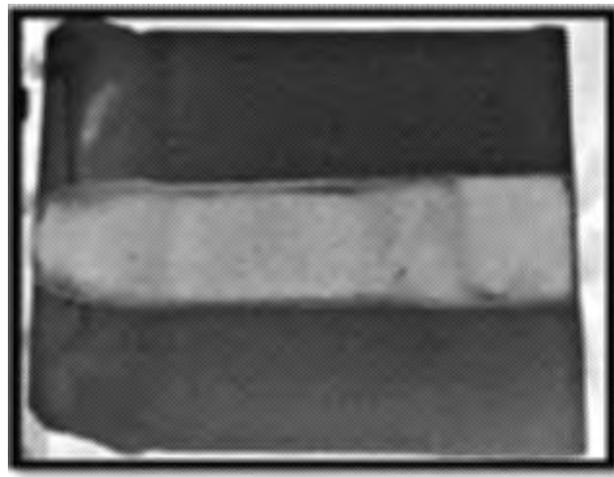Saline
Water

Brine

Porous Carbon Electrode

FIG. 1B
(Prior Art)

FIG. 2

FIG. 3

FIG. 4

FIG. 5

FIG. 6
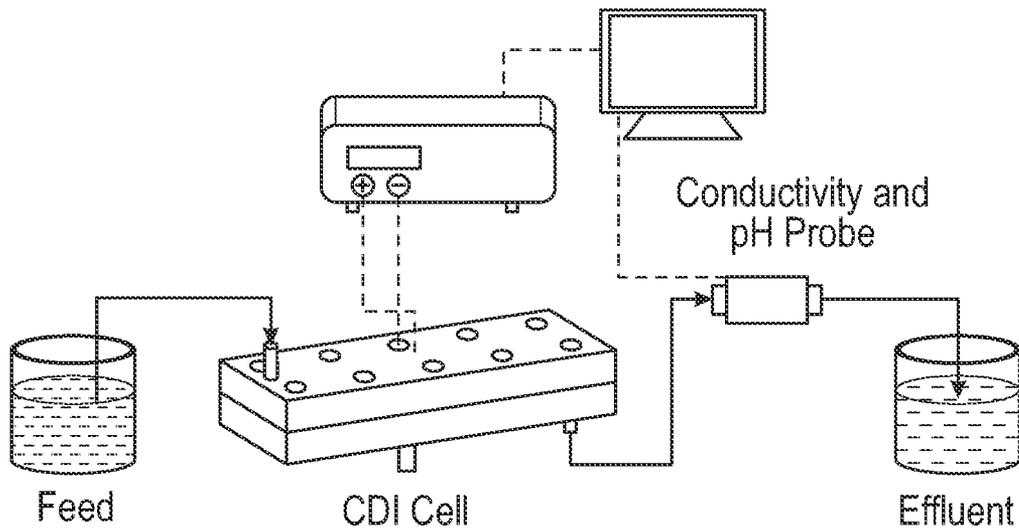
FIG. 7
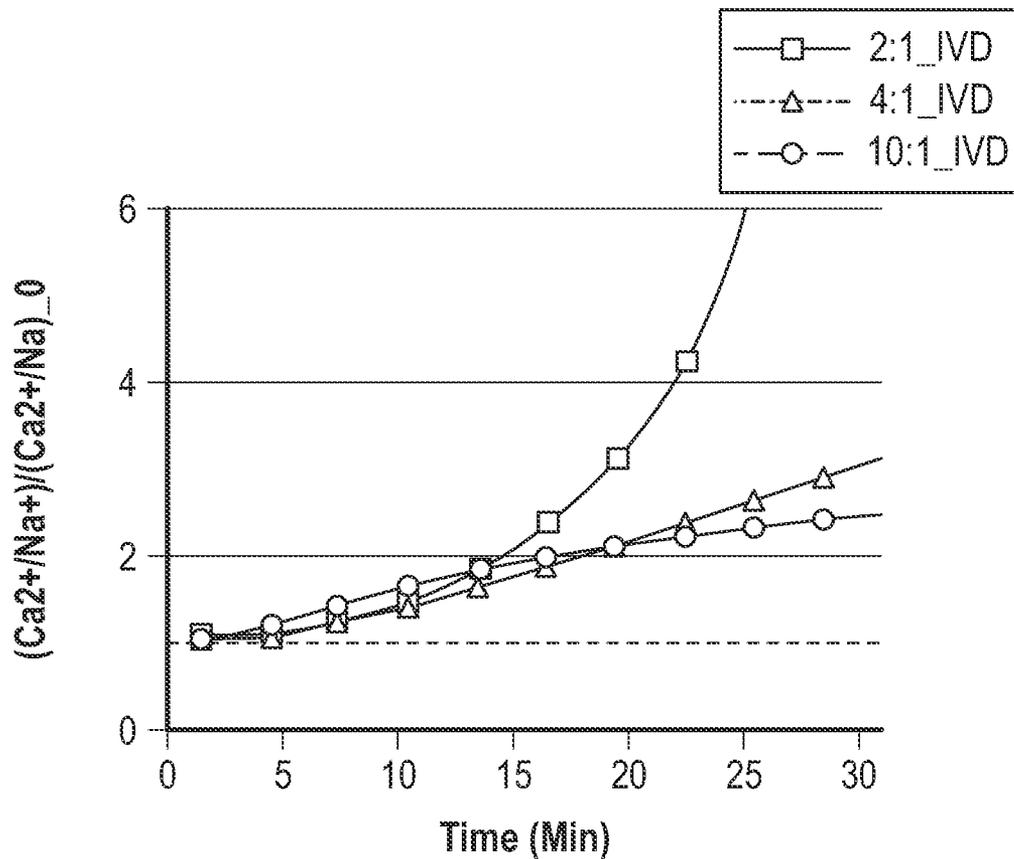
FIG. 8

FIG. 9

FIG. 10A

FIG. 10B

FIG. 10C

FIG. 11A

FIG. 11B

FIG. 11C

FIG. 11D

FIG. 12A

FIG. 12B

FIG. 12C

FIG. 12D

FIG. 13A

FIG. 13B
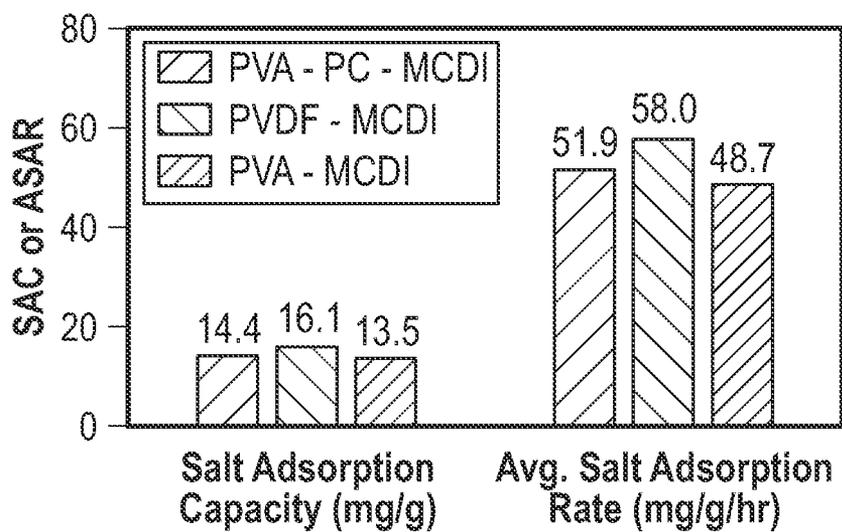
FIG. 13C
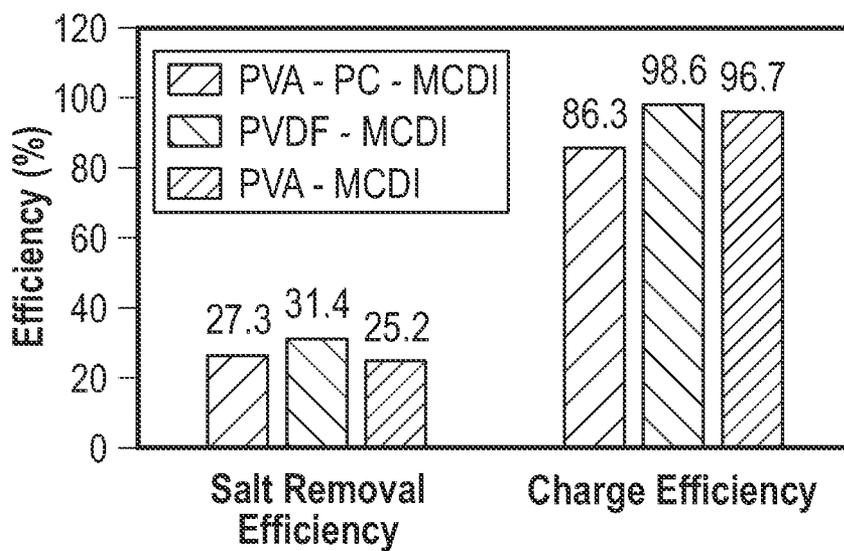
FIG. 13D

FIG. 14
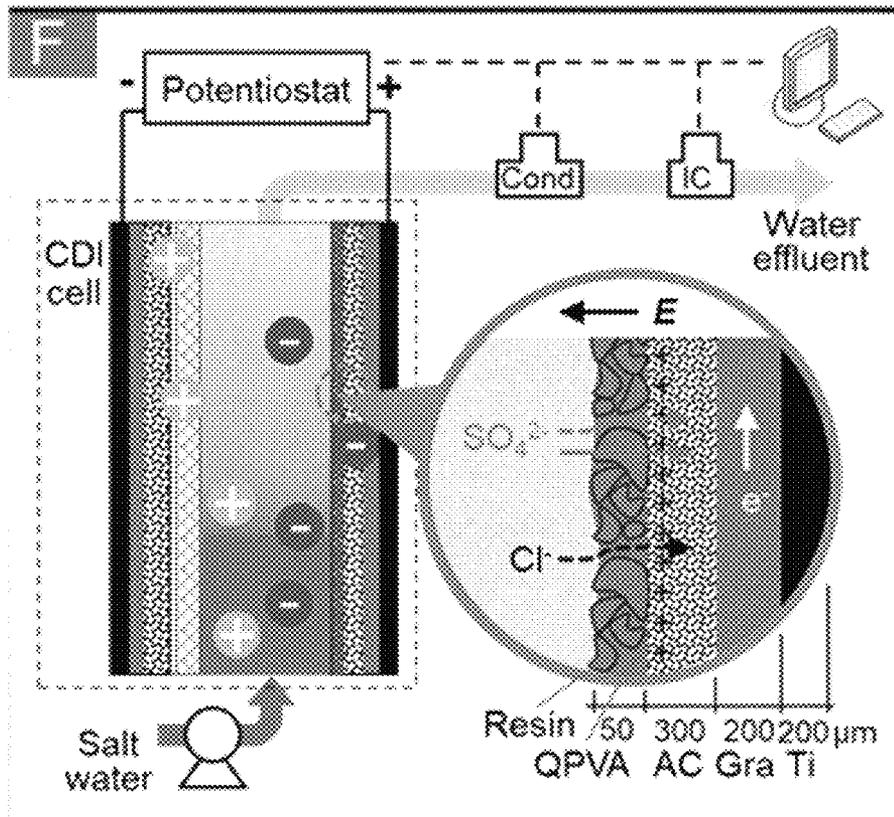
FIG. 15A
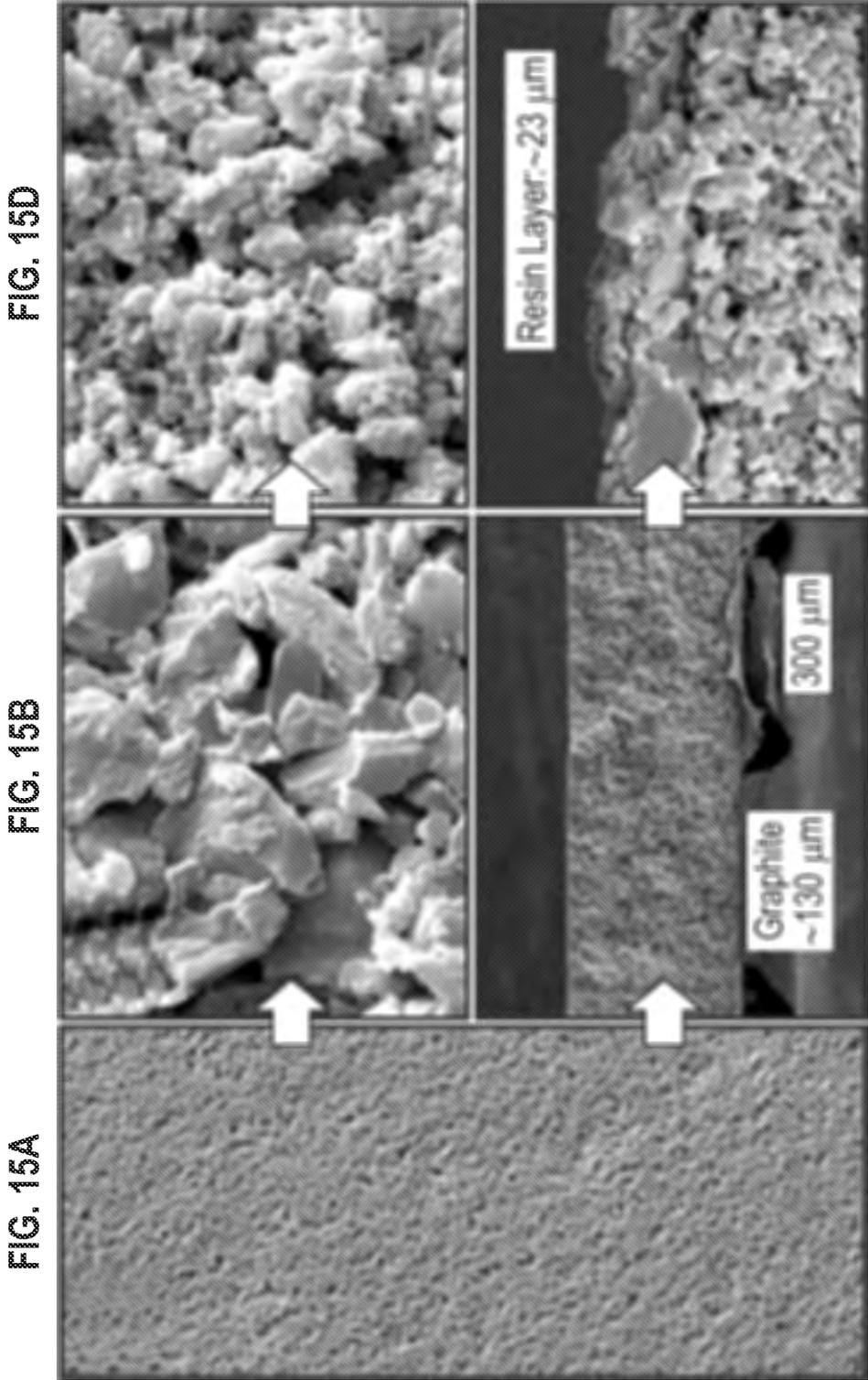
FIG. 15B

FIG. 15C

FIG. 15D

FIG. 15E

FIG. 15F

Fig. 16A

Fig. 16B

Fig. 16C

Fig. 16D

Fig. 16E

Fig. 17A

Fig. 17B

Fig. 17C

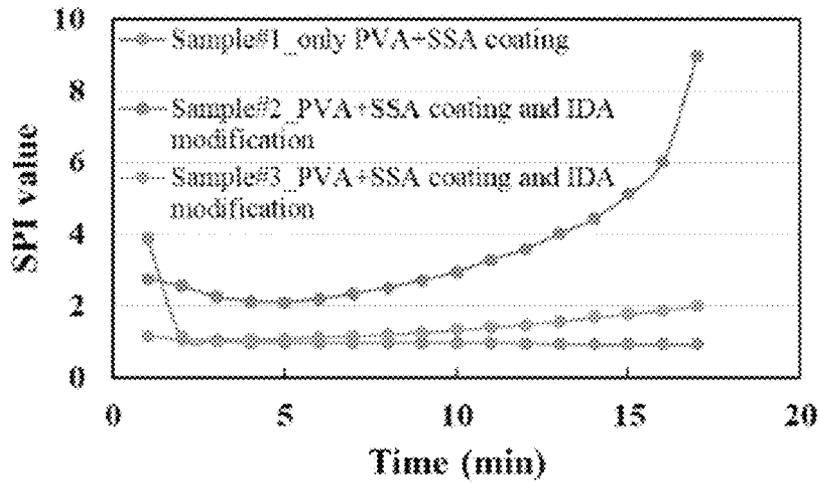Fig. 17D   Fig. 17E
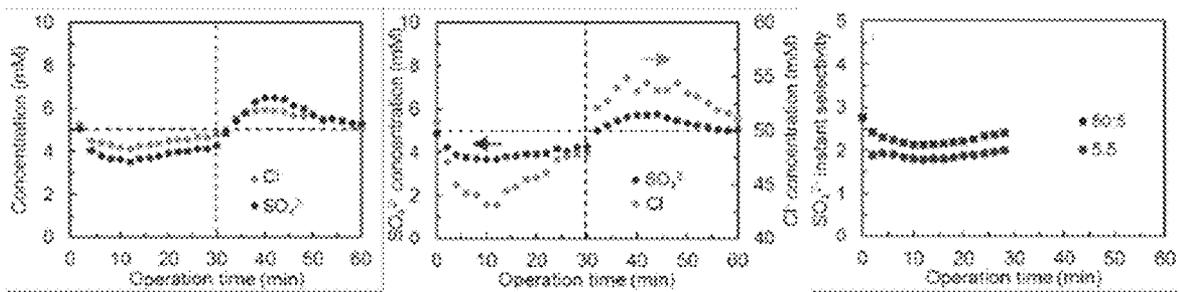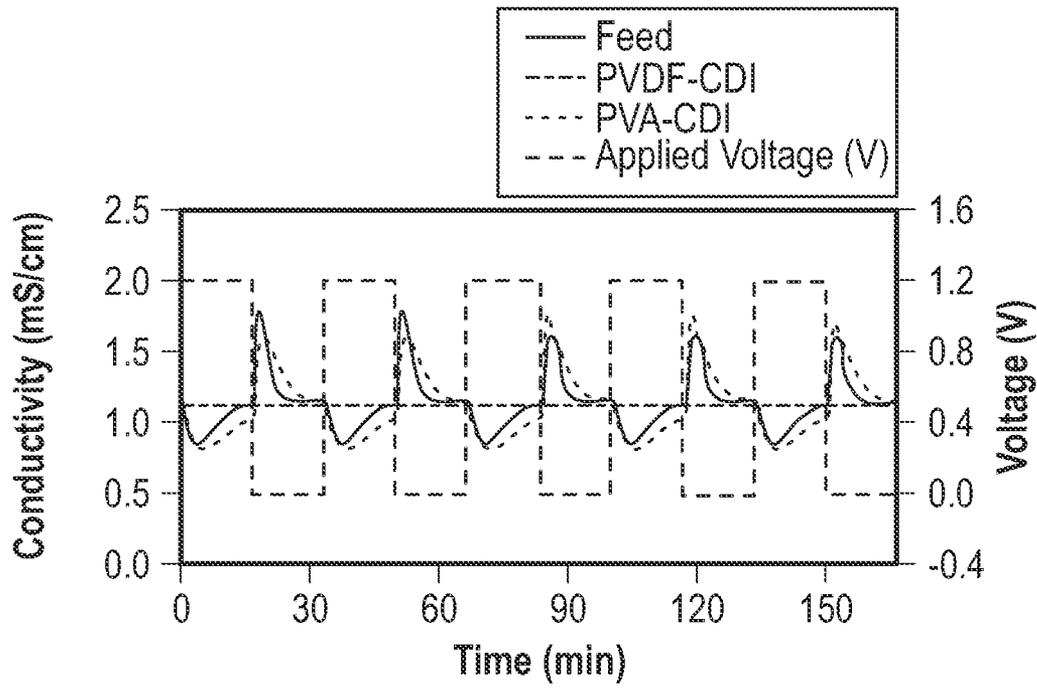
FIG. 18A

FIG. 18B

FIG. 18C

Fig. 19A
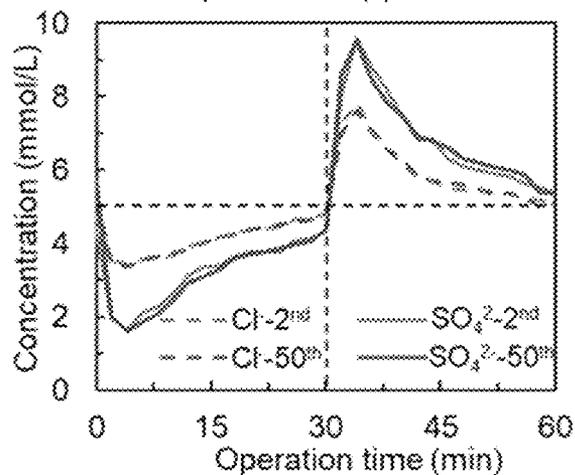
Fig. 19B

FIG. 20
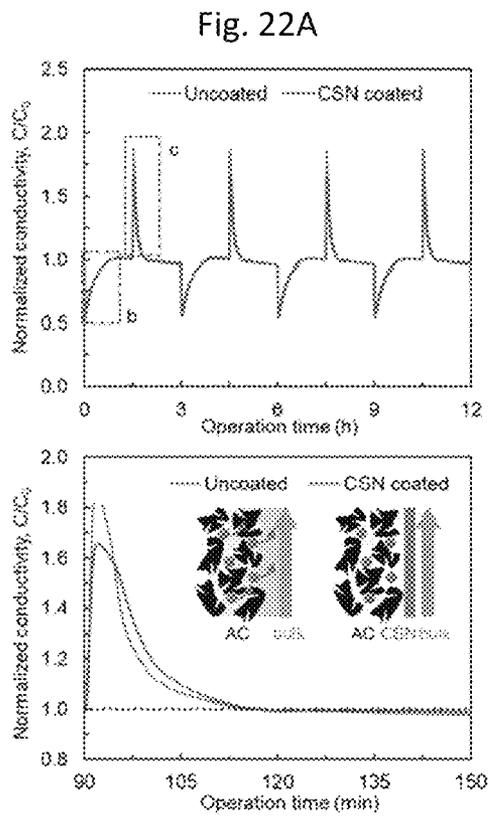
Fig. 21A
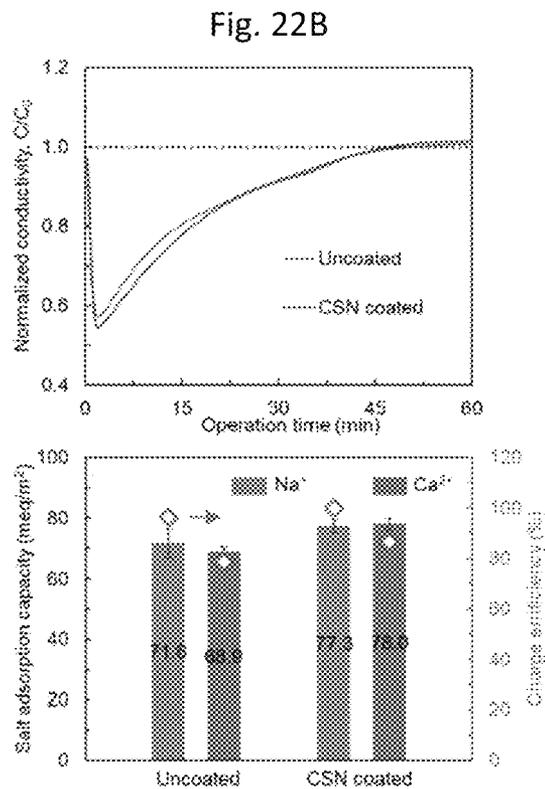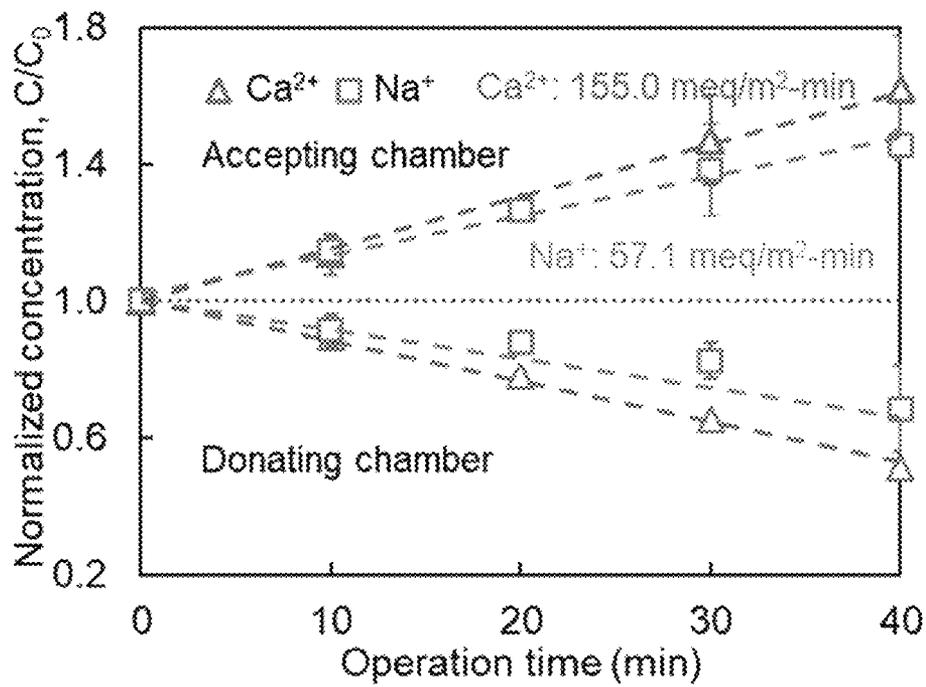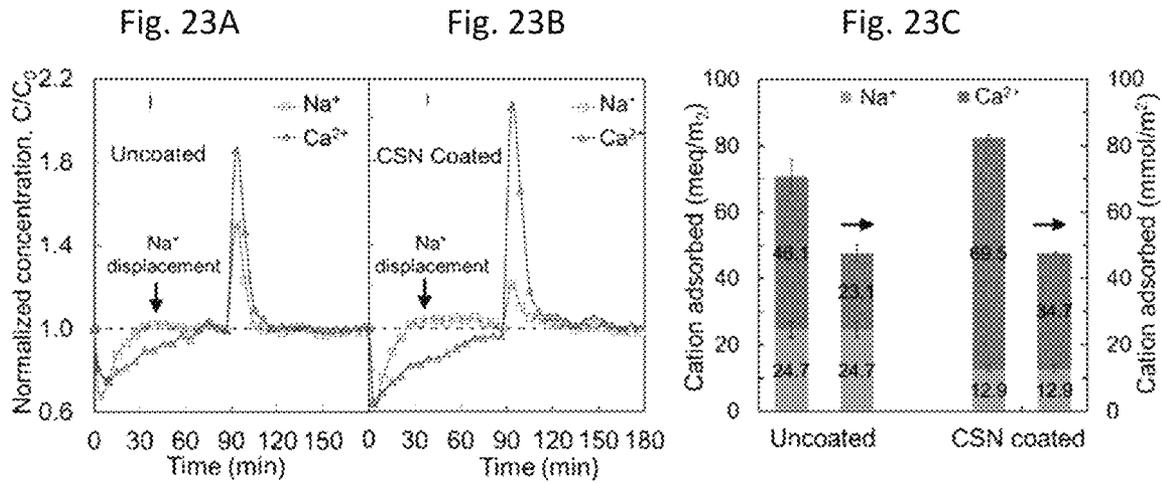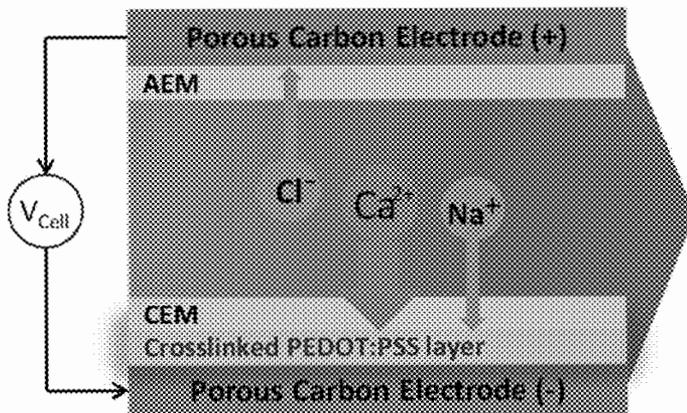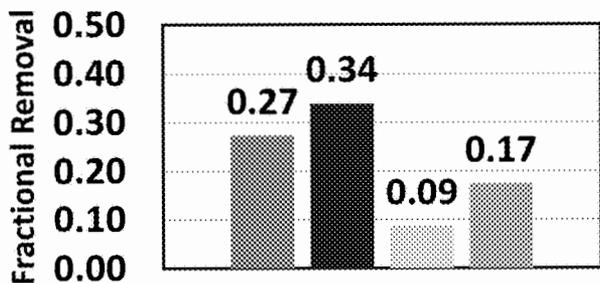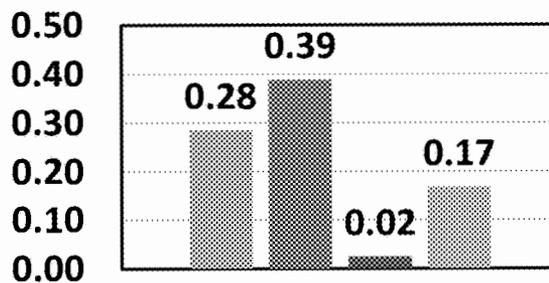
Fig. 21B
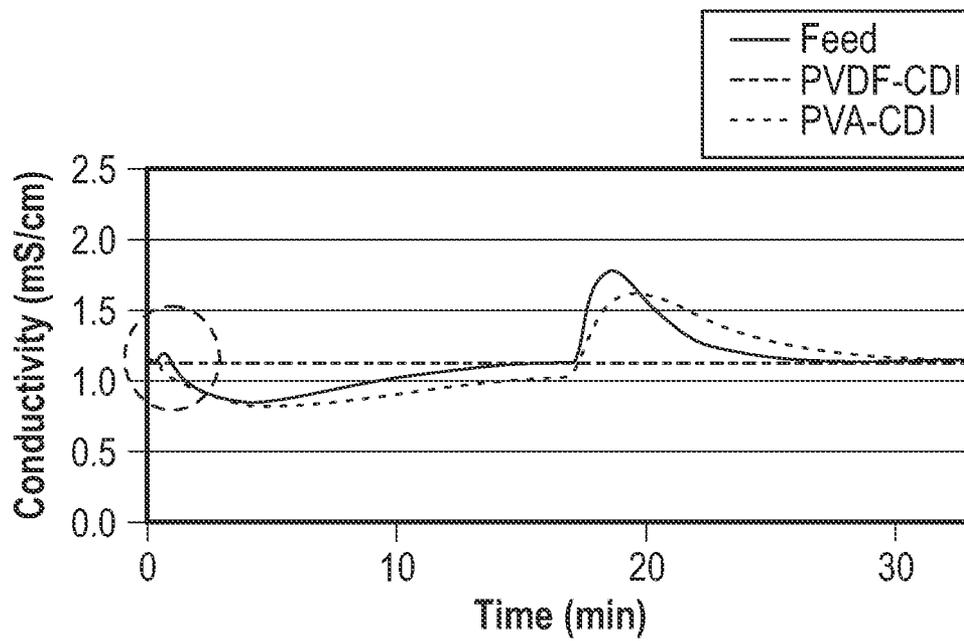
Fig. 21E
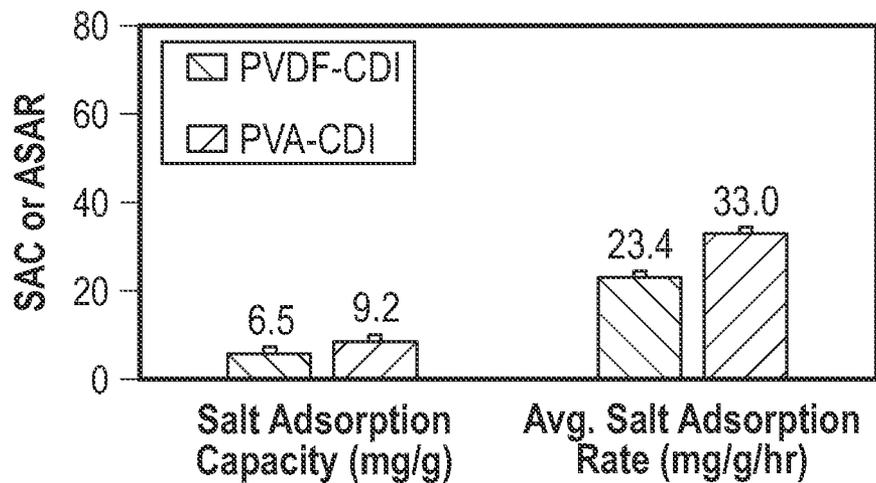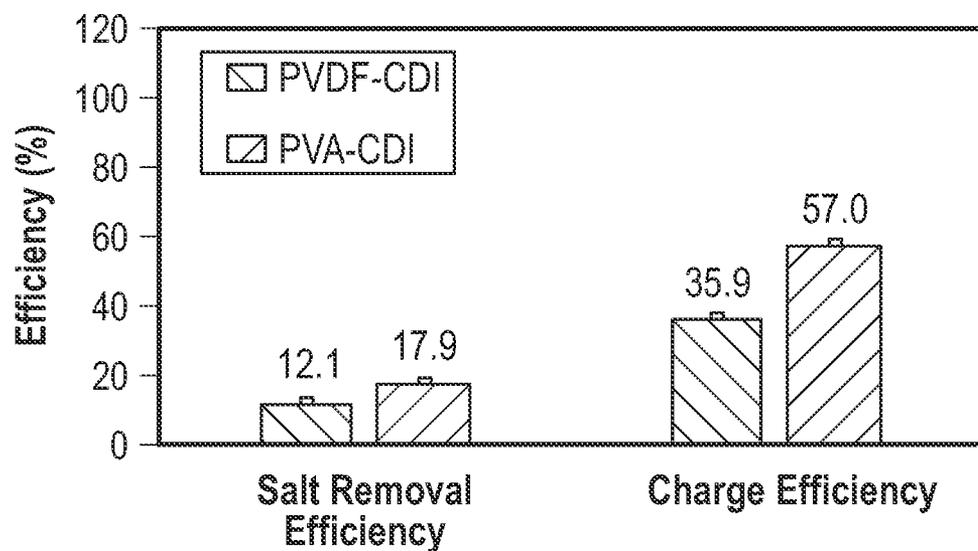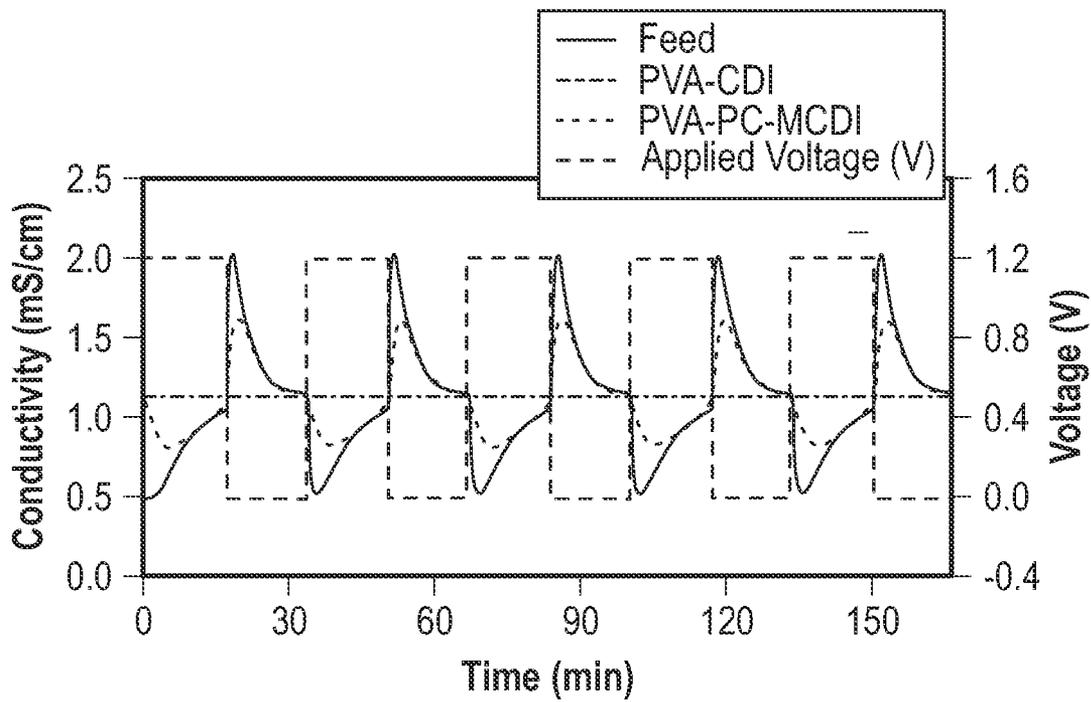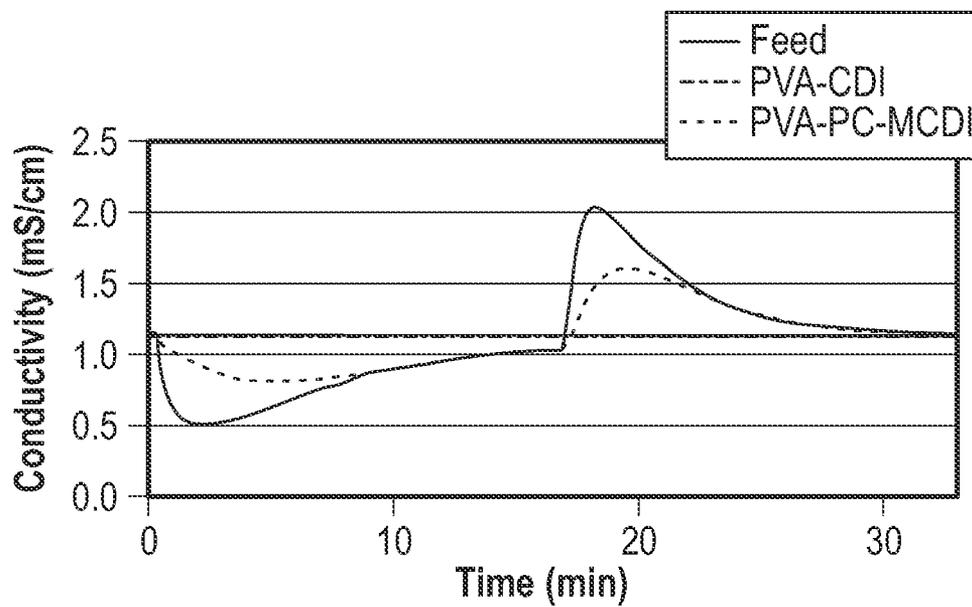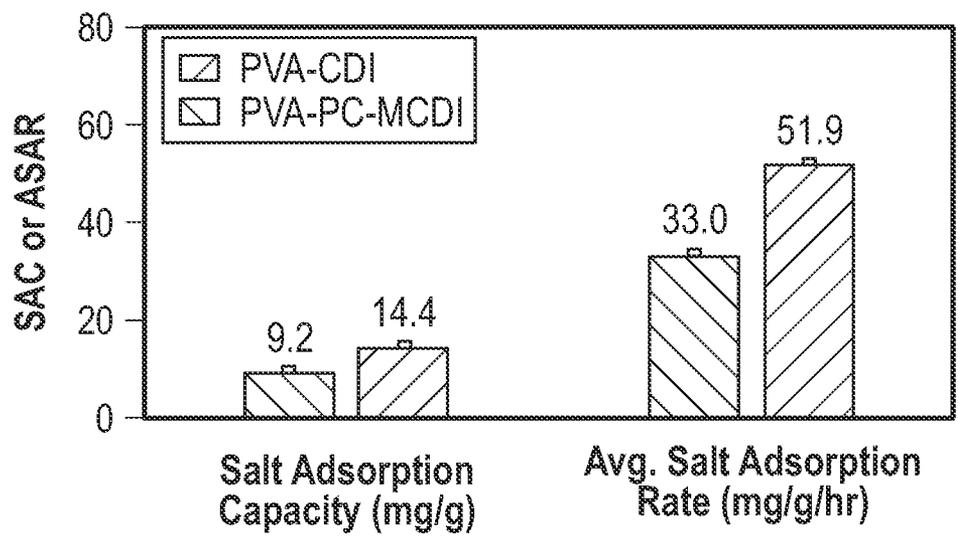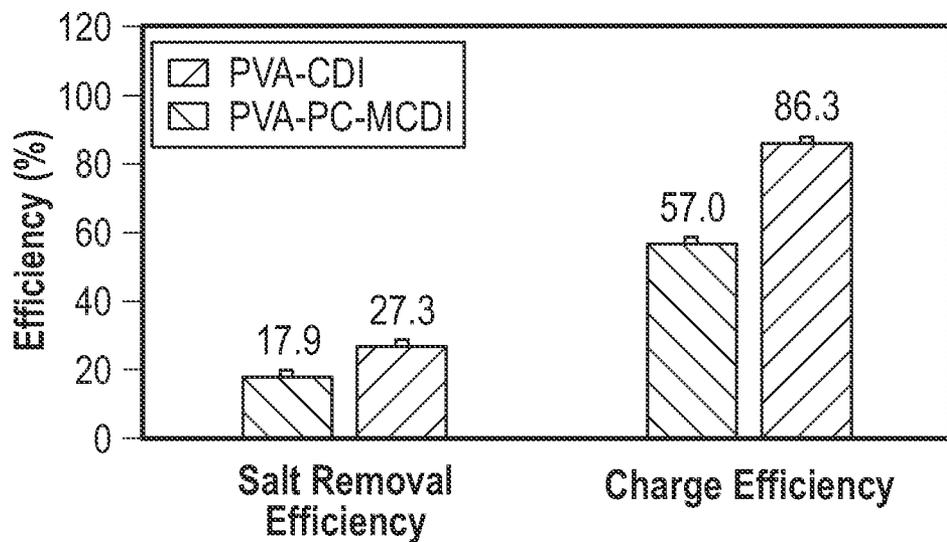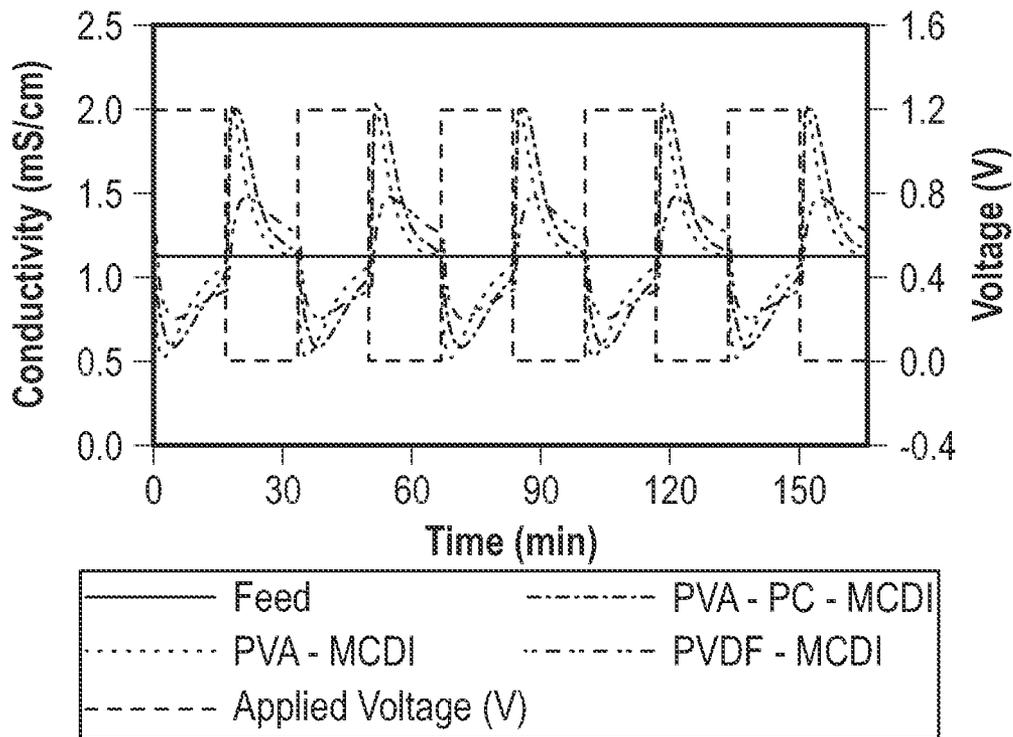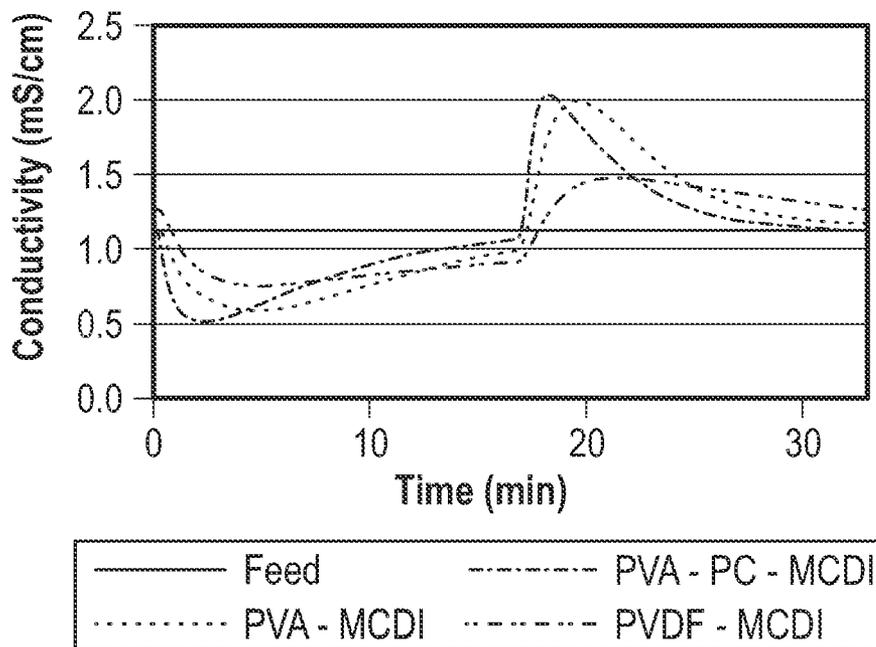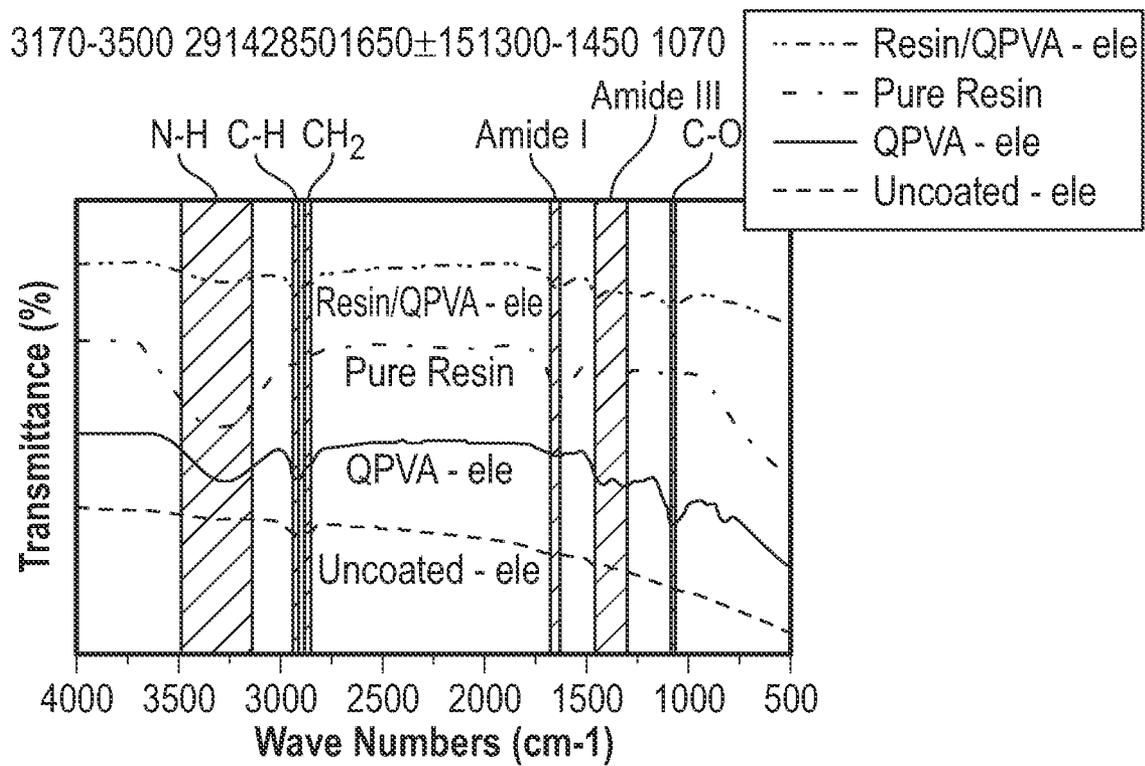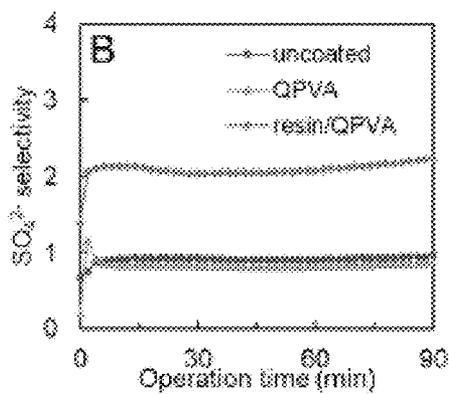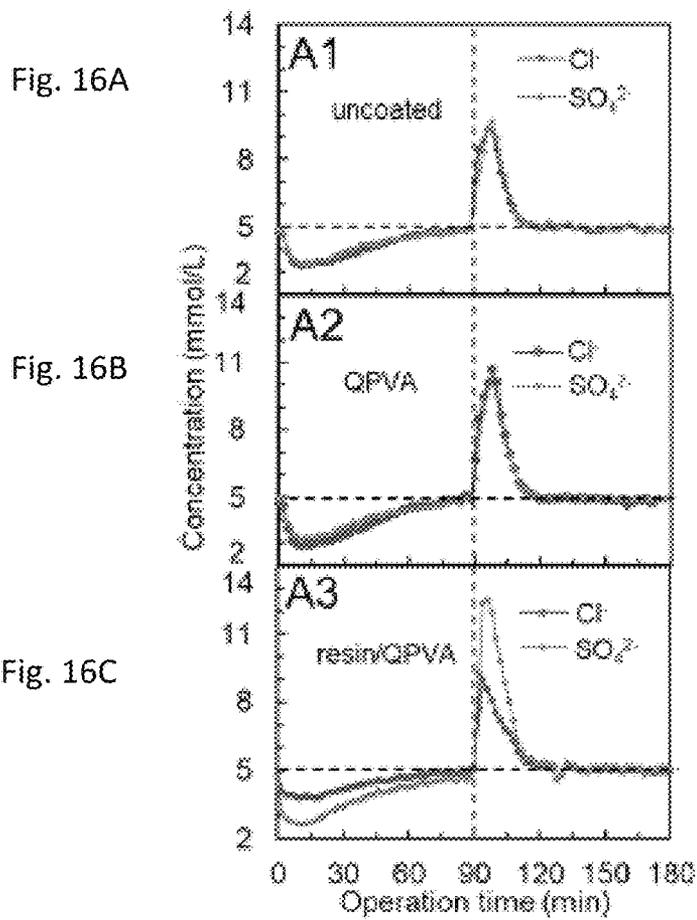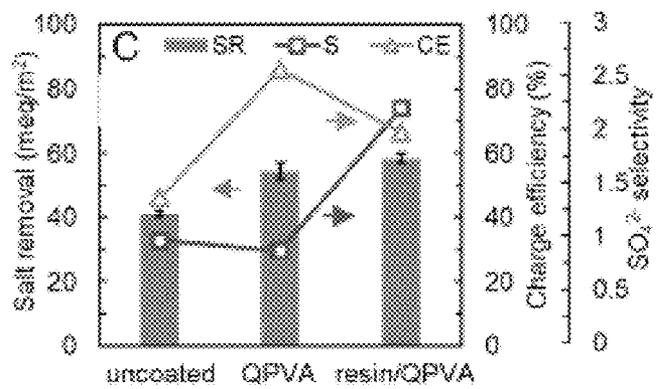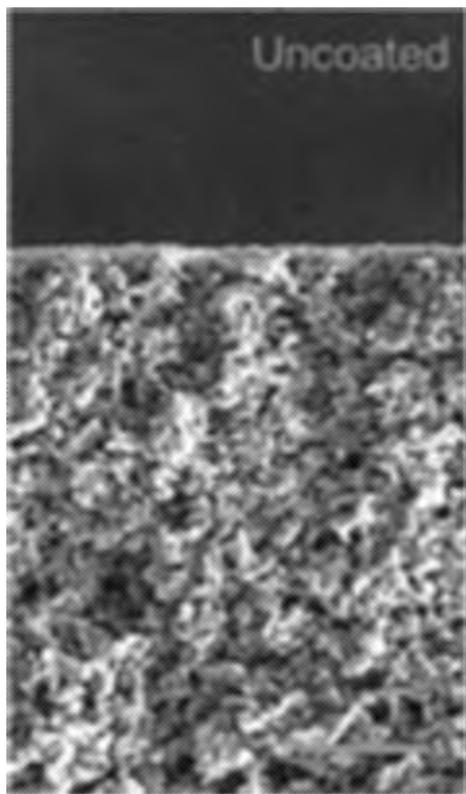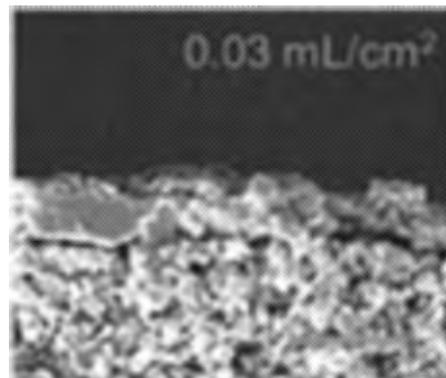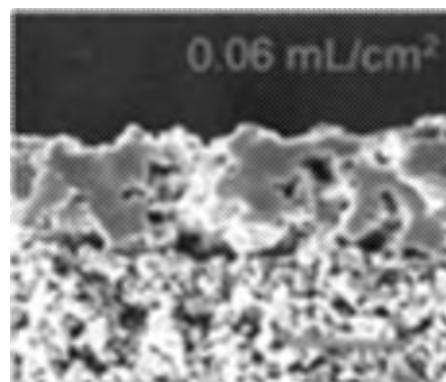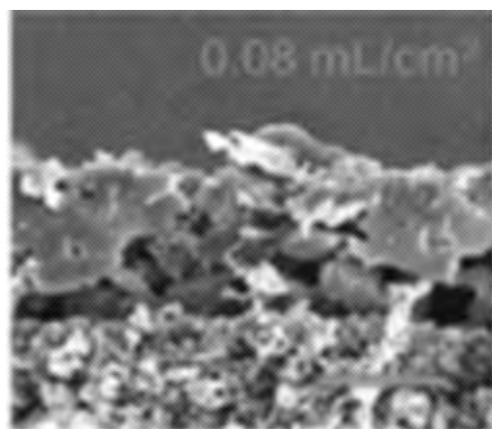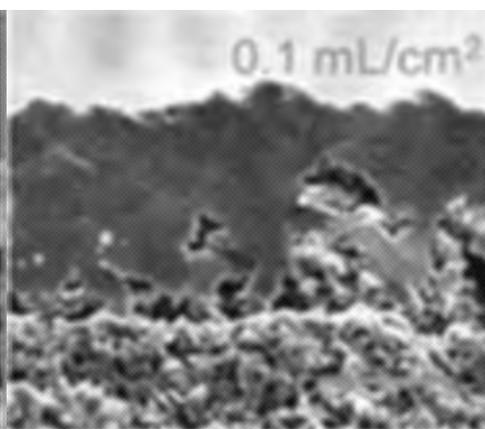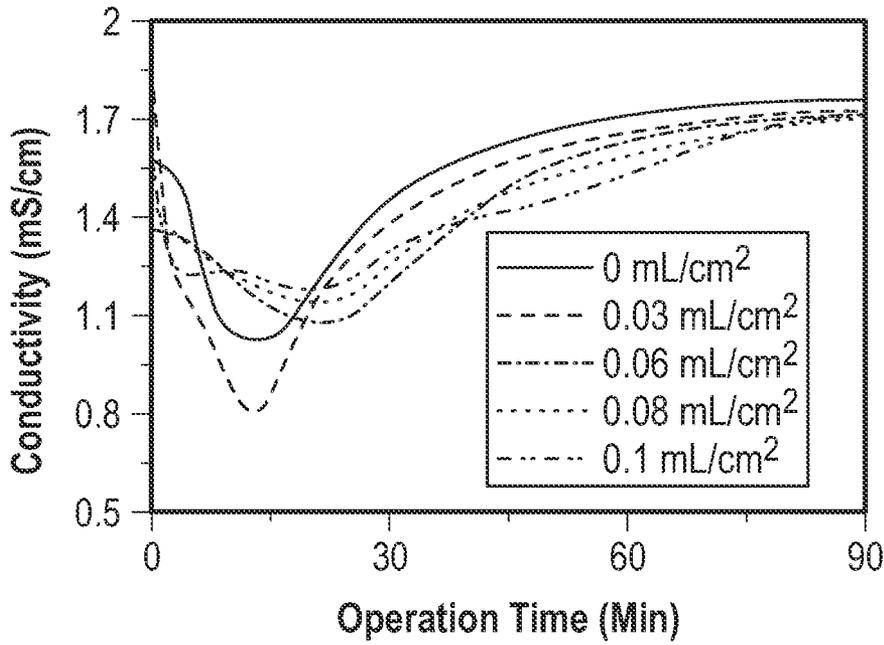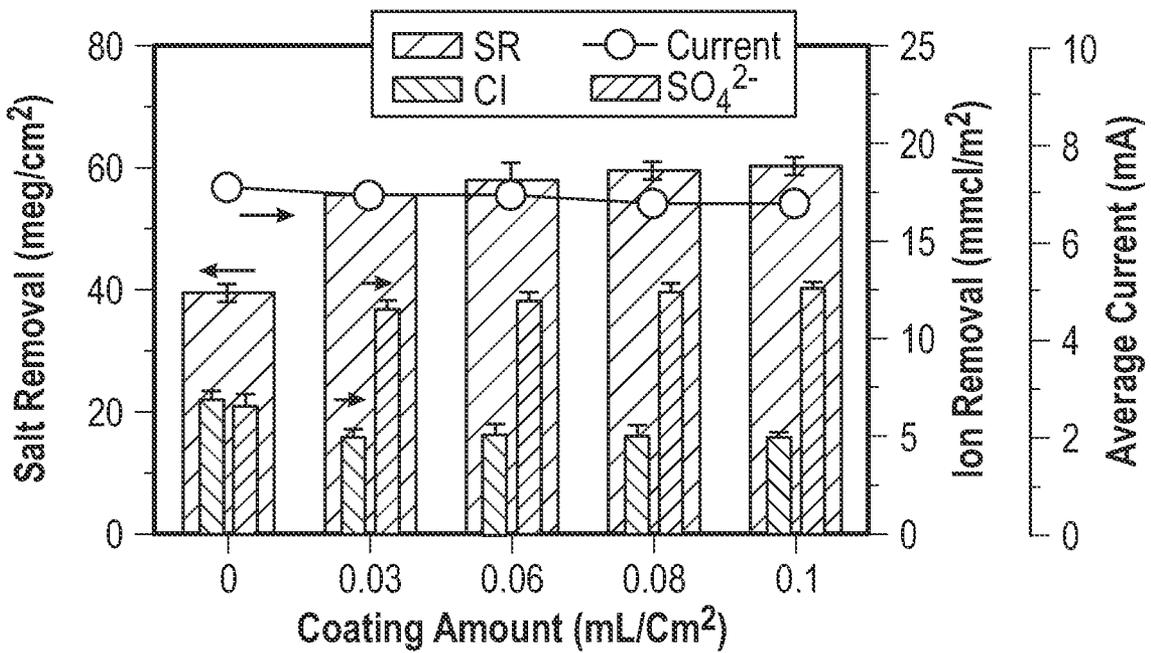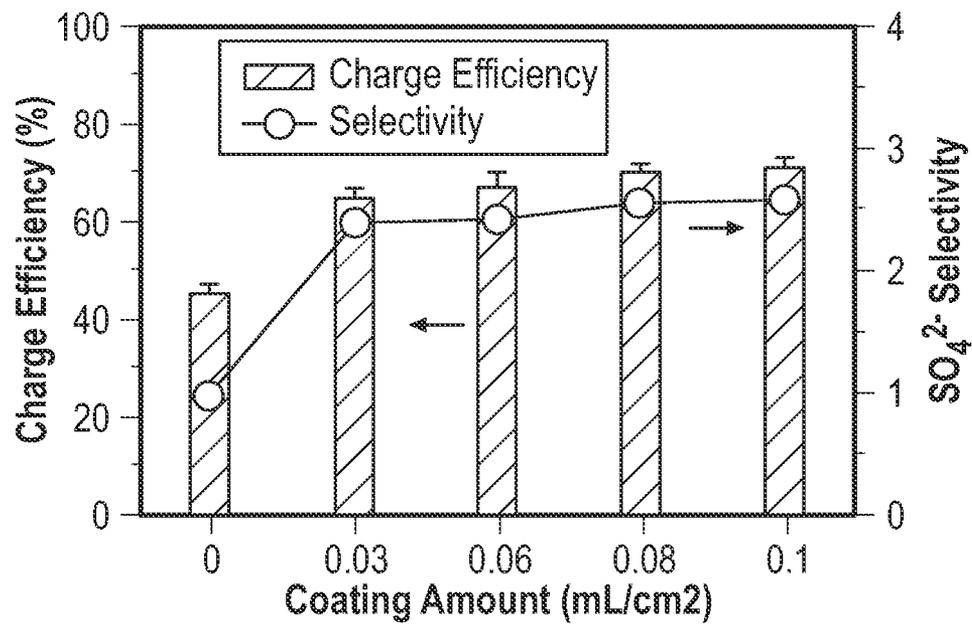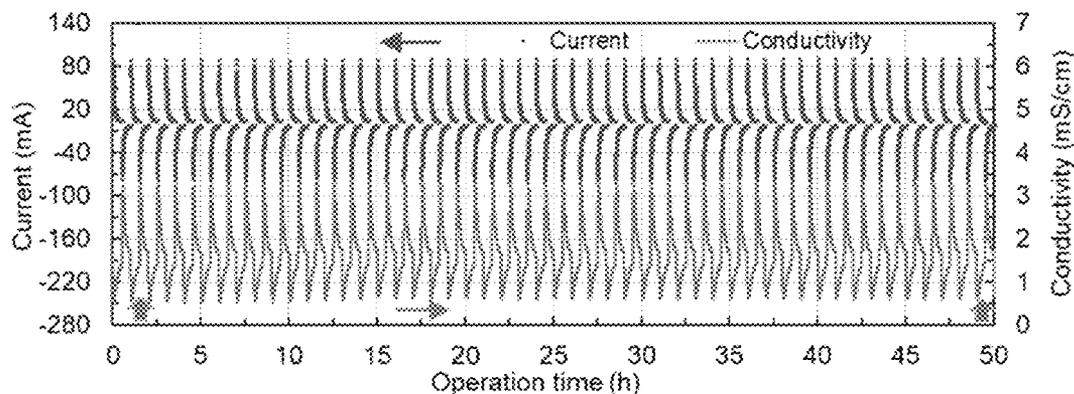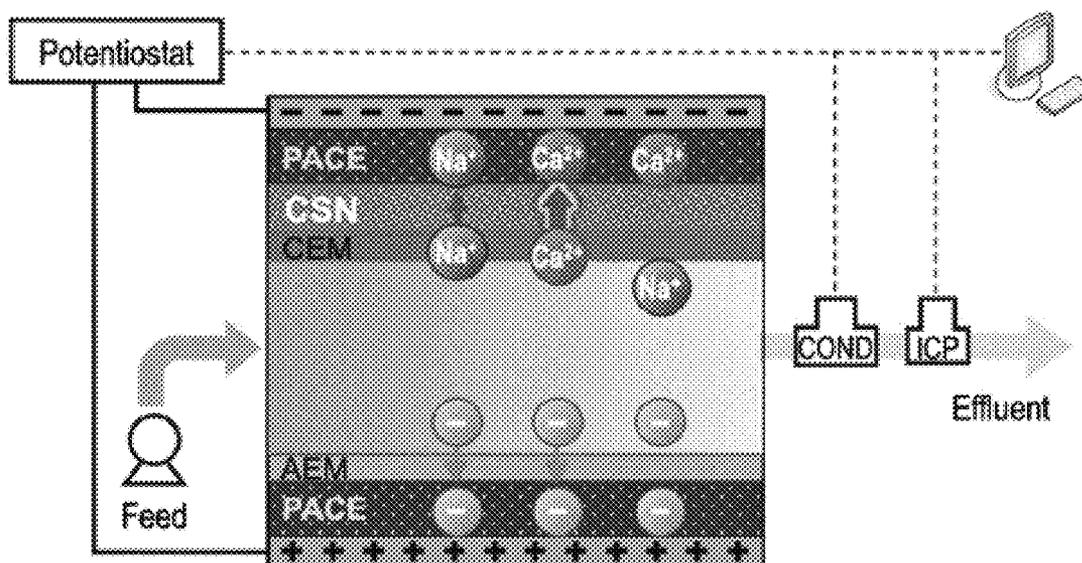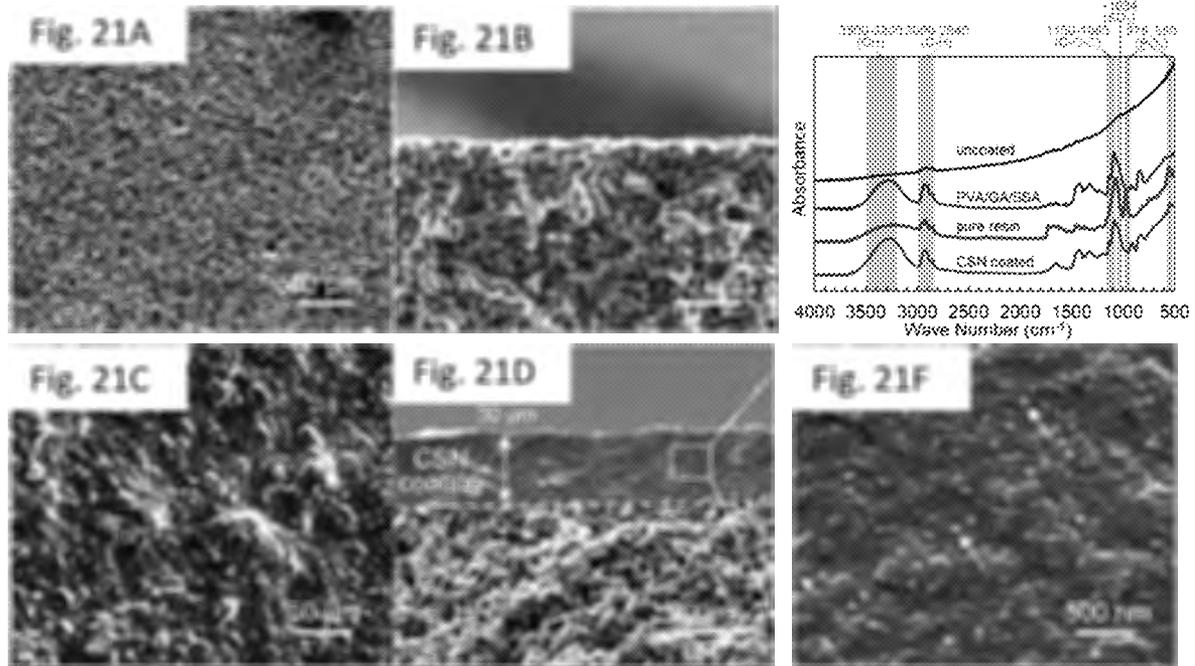
Fig. 21C

Fig. 21D

Fig. 21F

Fig. 22A

Fig. 22B

Fig. 22C

Fig. 22D

Fig. 23A   Fig. 23B   Fig. 23C

FIG. 24

Fig. 25

Fig. 26A

Fig. 26B
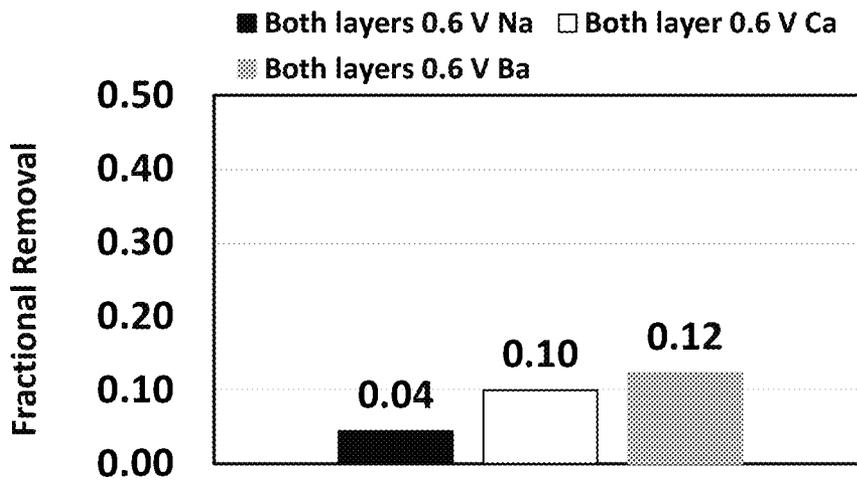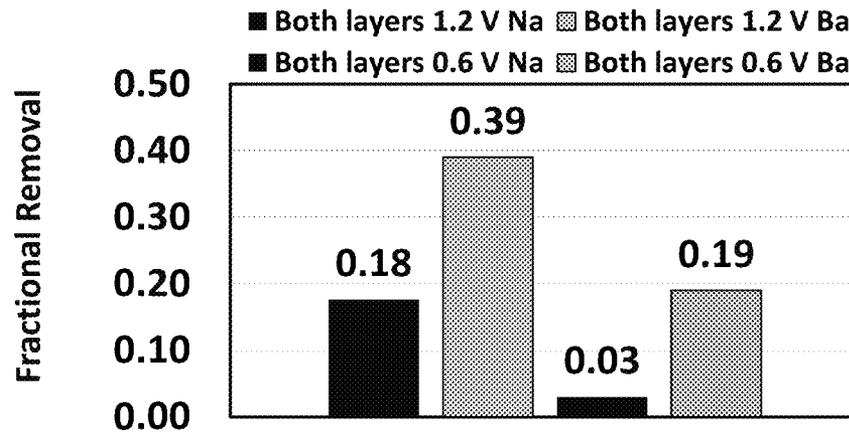
Fig. 27A

Fig. 27B

ELECTRODES FOR SELECTIVE REMOVAL OF MULTIVALENT IONS THROUGH CAPACITIVE DEIONIZATION

CROSS-REFERENCE TO RELATED APPLICATIONS

This Application claims the benefit of U.S. Provisional Application 62/715,116 filed on Aug. 6, 2018.

STATEMENT REGARDING FEDERALLY SPONSORED RESEARCH OR DEVELOPMENT

BACKGROUND

Capacitive deionization (CDI) is an approach for water desalination involving the reversible removal of ions by application of an electric potential between two electrodes. CDI is an emerging desalination technology that utilizes porous electrodes charged with a low electric potential to remove ionic species from aqueous solution through electrosorption. The electric field drives ions to the electrodes resulting in a stream of deionized water. CDI is a low-cost alternative desalination process to pressure based membrane desalination and thermal desalination methods. Ion-exchange membranes may be placed in front of the electrodes to prevent the passage of co-ions and improve the overall salt removal and charge efficiency. When the ion-exchange membranes are used, the process may be referred to as membrane capacitive deionization (MCDI).

The desalination performance and charge efficiency have also been improved through packing ion exchange resins or activated carbon between two electrodes to increase bulk conductivity, utilizing the flow through operation mode to enhance adsorption kinetics, optimizing electrical or hydraulic adsorption/desorption cycles, and coupling Faradaic pseudo capacitance.

In CDI, an electrical potential applied between porous electrodes drives the reversible electrosorption of ions. In MCDI, ion-exchange membranes are placed in front of the electrodes, as shown schematically in FIGS. 1A and 1B. The advantages of MCDI over CDI include an increase in the overall salt removal and charge efficiency due to blocking of co-ions and preventing or minimizing Faradaic reactions at the electrode surface that can degrade performance.

CDI has been studied for desalination of seawater, brackish water, and domestic wastewater. It has also been coupled with other processes such as microbial fuel cells and filtration membranes. The adsorption capacity of CDI electrodes has grown from less than 3 to more than 30 mg NaCl per gram of electrode.

SUMMARY

This summary is provided to introduce a selection of concepts that are further described below in the detailed description. This summary is not intended to identify key or essential features of the claimed subject matter, nor is it intended to be used as an aid in limiting the scope of the claimed subject matter.

In one aspect, embodiments disclosed herein relate to a method of forming an electrode for capacitive deionization that includes depositing an slurry onto a substrate, wherein the slurry comprises a porous material, a first crosslinkable hydrophilic polymer, and a crosslinker for the first crosslinkable hydrophilic polymer; annealing the slurry deposited on the substrate to create a crosslinked porous layer on the substrate; depositing an solution comprising an ion-exchange material, a second crosslinkable hydrophilic polymer, and a crosslinker for the second crosslinkable hydrophilic polymer onto the crosslinked porous layer; and optionally annealing and/or drying the solution on the crosslinked porous layer.

In another aspect, embodiments disclosed herein relate to a method of deionizing an aqueous fluid that includes continuously flowing the aqueous fluid through a capacitive deionization reactor that includes at least one electrode fabricated according to methods described herein while applying a voltage between an anode and a cathode of the capacitive deionization reactor.

In another aspect, embodiments disclosed herein relate to a method of deionizing an aqueous fluid that includes continuously flowing the aqueous fluid through a capacitive deionization reactor that includes at least one electrode fabricated to selectively remove a targeted ion, while applying a voltage between an anode and a cathode of the capacitive deionization reactor.

In yet another aspect, embodiments disclosed herein relate to an apparatus for capacitive deionization reactions that includes a cathode, and an anode, wherein at least one of the anode and/or cathode is a crosslinked porous electrode formed by the method of claim 1. The apparatus further includes wherein the crosslinked porous electrode comprises substrate, a first porous layer deposited on the substrate, and a second layer deposited on the first porous layer; wherein the first porous layer comprises a porous material and a crosslinked hydrophilic polymer, and the second layer comprises an ion exchange material, a crosslinked or non-crosslinked hydrophilic polymer, and optionally a crosslinker.

Other aspects and advantages of the claimed subject matter will be apparent from the following description and the appended claims.

BRIEF DESCRIPTION OF DRAWINGS

FIGS. 1A-1B show a schematic for MCDI operation during (FIG. 1A) ion uptake and (FIG. 1B) ion desorption.

FIG. 2 shows a schematic illustrating the concept of selective cation removal.

FIG. 3 shows a flow coating setup and flow coating mechanism with a movable stage.

FIG. 4 shows a schematic of the modification procedure for modifying a PVA+SSA/GA coated electrode with IDA.

FIG. 5 shows a schematic for MCDI cell assembly.

FIG. 6 shows an image of a PVA/GA selective nanosorbent anion exchange resin coated electrode where the resin comprises milled anion exchange nanoparticles.

FIG. 7 shows a schematic of a lab scale CDI set up.

FIG. 8 shows the selective ion removal for the three electrodes compared in Study 1.

FIG. 9 shows a graph of the selective ion removal for electrodes coated with PVA and SSA both with and without IDA modification.

FIGS. **10A-10C** show the removal behavior and selectivity of multiple ions by a resin coated CDI reactor. FIG. **10A** shows ion selectivity for a concentration of Cl⁻ and SO₄²⁻ with a Cl⁻/SO₄²⁻ concentration of 5:5; (FIG. **10B**) concentration of Cl⁻ and SO₄²⁻ with a Cl⁻/SO₄²⁻ concentration of 50:5; (FIG. **10C**) instant selectivity of SO₄²⁻ over Cl⁻ during adsorption period.

FIGS. **11A-11D** show a performance comparison of CDI systems comprising electrodes prepared in accordance with Example 1 (PVA-CDI) and Example 2 (PVDF-CDI). FIG. **11A** shows effluent conductivity over 5 cycles of operation; FIG. **11B** shows effluent conductivity over 1 cycle showing the inversion effect for an electrode of Example 2 at the onset of the adsorption cycle (indicated by the circle); FIG. **11C** shows a comparison of the PVA and PVDF CDI systems ability to remove or adsorb ions from solution; and FIG. **11D** shows salt removal and charge efficiencies for both systems.

FIGS. **12A-12D** show a performance comparison of CDI and MCDI systems comprising electrodes prepared in accordance with Example 1 (PVA-CDI) and Example 3 (PVA-PC-MCDI). FIG. **12A** shows effluent conductivity over 5 cycles of operation; FIG. **12B** shows effluent conductivity over 1 cycle showing greater uptake for an electrode of Example 3; FIG. **12C** shows a comparison of the PVA-CDI and PVA-PC-MCDI systems ability to remove or adsorb ions from solution; and FIG. **12D** shows salt removal and charge efficiencies for both systems comparatively.

FIGS. **13A-13D** show a performance comparison of CDI and MCDI systems comprising electrodes prepared in accordance with Example 1 (PVA-MCDI) and Example 3 (PVA-PC-MCDI) and PVDF-MCDI. FIG. **13A** shows effluent conductivity over 5 cycles of operation; FIG. **13B** shows effluent conductivity over 1 cycle showing greater uptake for an electrode of Example 3; FIG. **13C** shows a comparison of the PVA-MCDI, PVA-PC-MCDI, and PVDF-MCDI systems ability to remove or adsorb ions from solution; and FIG. **13D** shows salt removal and charge efficiencies of the three systems comparatively.

FIG. **14** shows a schematic diagram of a CDI operation system with an activated carbon electrode on graphite, and a selective nano-sorbent resin/QPVA coating on the activated carbon electrode.

FIGS. **15A-F** show (FIGS. **15A-15C**) SEM images of surface and cross-sections of an uncoated carbon electrode; while FIGS. **15D** and **15E** show SEM images of surface and cross-sections of a selective nano-sorbent resin/QPVA coated electrode, respectively. FIG. **15F** shows an FTIR spectra of the different electrode materials. PAC: powered activated carbon; ele: activated carbon electrode.

FIGS. **16A-16E** show desalination performance and ion removal in uncoated, QPVA coated, and selective nano-sorbent resin/QPVA coated electrode. FIG. **16A-16C** show the concentration change of Cl⁻ and SO₄²⁻ during an adsorption and desorption cycle for each electrode; while FIG. **16D** shows SO₄²⁻ selectivity during adsorption period; and FIG. **16E** shows salt removal (SR), charge efficiency (CE), and SO₄²⁻ selectivity (S) of the three electrodes. Arrows in panel A and C represent corresponding axis.

FIGS. **17A-17E** show SEM images of carbon electrodes coated with various amounts of selective nano-sorbent resin slurry as noted in the images. The scale bar in panel A represents 40 μm.

FIGS. **18A-18C** show the influence of coating thickness (coating amount) on CDI performance. FIG. **18A** shows conductivity of CDI effluent during adsorption period; (FIG. **18B**) total salt removal, current production, and anion

removal during adsorption period; and (FIG. **18C**) charge efficiency and SO₄²⁻ selectivity. Arrows in panel C and D represent corresponding axis.

FIGS. **19A-19B** show the long-term stability of the selective nano-sorbent resin/QPVA coated electrode during 50 cycles of operation. FIG. **19A** shows current and conductivity of CDI effluent; FIG. **19B** shows Cl⁻ and SO₄²⁻ evolution during the 2nd and 50th cycle.

FIG. **20** shows a schematic diagram of the experimental setup used in Study 4. (CSN: Ca2⁺ selective nanocomposite, PACE: powdered activated carbon electrode; COND: conductivity sensor; ICP: inductively coupled plasma spectroscopy).

FIGS. **21A-21F** show SEM images wherein the top (FIG. **21A**) and cross-sectional view (FIG. **21B**) are of uncoated electrode, and top (FIG. **21C**) and cross-sectional view (FIG. **21D**, **21F**) of the CSN electrode; arrows in FIG. **21F** indicating resin nanoparticles. FIG. **21E** shows FTIR spectra of uncoated, PVA/GA/SSA-coated, pure resin, and the— CSN coated electrode.

FIGS. **22A-22D** show (FIG. **22A**) conductivity profiles of the two electrodes; (FIG. **22B**) conductivity profile during one adsorption stage; (FIG. **22C**) conductivity profile during one desorption stage, with insert illustrating desorption at a microscopic scale; and (FIG. **22D**) salt adsorption capacity and charge efficiency of uncoated and CSN electrodes in single NaCl or CaCl₂ solution.

FIGS. **23A-23C** show (FIG. **23A-23B**) concentration profiles of Na⁺ and Ca²⁺ during an adsorption/desorption cycle using the uncoated (FIG. **23A**) and CSN coated (FIG. **23B**) electrodes at an initial Na⁺-to-Ca²⁺ equivalent ratio of 1:1; (FIG. **23C**) cations adsorbed by uncoated and CSN electrodes at an influent Na⁺-to-Ca²⁺ equivalent ratio of 1:1.

FIG. **24** shows Ion-transport of Na⁺ and Ca²⁺ through the CSN layer in the electro-dialysis experiment.

FIG. **25** shows a schematic diagram of an MCDI operation system with an activated carbon electrode on graphite, and a crosslinked PEDOT:PSS coating on the activated carbon electrode.

FIGS. **26A-26B** show a comparative graph of the fractional removal ratio of Na⁺ and Ca²⁺ for electrodes comprising only a CEM (FIG. **26A**) and for electrodes comprising a CEM in addition to a PEDOT:PSS crosslinked layer (FIG. **26B**).

FIGS. **27A-27B** show a comparative graph of the fractional removal ratio of Ba²⁺ and Ca²⁺ for electrodes comprising both layers CEM (FIG. **27A**) at different applied voltages and FIG. **27B** shows the fractional removal ratio of each ion from a mixed solution comprising all three (Na⁺, Ca²⁺, Ba²⁺).

DETAILED DESCRIPTION

Embodiments disclosed herein relate generally towards ion selective polymer coated electrodes and methods of making and using the same in CDI or MCDI devices. For ease of reading "CDI" and "MCDI" will be used interchangeably herein, and the ion selective polymer coated electrodes described herein may be utilized in either process. The ion selective polymer coated electrodes may be used in MCDI devices to selectively remove multivalent cations and/or anions. The desalination performance and charge efficiency may be improved through packing ion exchange resins or activated carbon between two electrodes to increase bulk conductivity, utilizing the flow through operation mode to enhance adsorption kinetics, optimizing elec-

trical or hydraulic adsorption/desorption cycles, and coupling Faradaic pseudo capacitance.

More than one embodiment presented herein may relate to electrodes fabricated for deionization processes. However, it should be noted that such electrodes prepared in accordance with one or more embodiments presented herein may be used in a variety of electrosorption applications.

Electrodes used in CDI and MCDI may be comprised of a porous active material, an optional conductive additive, polymeric binder, and optional ion-exchange polymeric coatings wherein the ion-exchange coating may comprise selective ion-exchange nanoparticles. Significant work has been focused on the development of highly-porous active materials to increase charge storage capacities so that the ion removal capacity may be increased. However, conventional desalination and/or capacitive deionization processes do not have any selectivity for multivalent ions, which are commonly the most problematic as they are corrosive and contribute significantly to fouling and scaling of surfaces, membranes, pipes, etc.

Ion selective polymer coated electrodes disclosed herein may be used to selectively remove harmful/undesirable ionic contaminants from aqueous fluids (e.g., drinking water), as shown in FIG. 2. For example, some harmful/undesirable ions may include heavy metals, fluoride, and oxyanions. More specifically, some harmful/undesirable ions may include, but are not limited to, chromate, sulfate, Li^+, Sr^{2+}, Ca^{2+}, Ba^{2+}, Cu^{2+}, Pb^{2+}, $As(V)$, $Cr(VI)$, and NO_3^-. In one or more embodiments, the ion selective electrodes may have tailored chemical compositions that can target specific contaminants for preferential removal during CDI processes.

Further, the material for polymeric binder and/or ion-exchange polymer coating in electrodes plays an important role in determining ion permeability and mechanical properties of electrodes in CDI processes. The material selection for the binder and the polymer coating also influences the solvents that can be used during the fabrication and processing of CDI electrodes. Polymeric binding material used to fabricate electrodes may include, for example, poly (vinylidene fluoride) (PVDF) or polytetrafluoroethylene (PTFE) organic polymers which are insoluble in water. In many cases, CDI fabrication methods may use organic solvents to solubilize the PVDF and/or PTFE binders. Moreover, solvents may also be used for processing ion-exchange polymer coatings, as they may find use for solubilizing the polymer resins used in the coating.

Significantly, the organic solvents used in conventional CDI fabrication techniques may not be completely removed during fabrication (even after a drying process), and thus residual organic solvents have the potential to leach out during operation of the system, thereby contaminating the de-ionized fluid product and potentially adversely impacting the drinking water application of such systems. Thus, an alternative process for fabricating electrodes and ion-exchange layers for MCDI that does not rely on organic solvents would be desirable to simplify the fabrication process, reduce electrode size and weight, and avoid the use of organic solvents. The ion-selective electrodes described herein may be fabricated using a purely water-based process (i.e., no organic solvents used for both binder and coating), and therefore are safer and more environmentally friendly.

One or more embodiments herein relate to preparing ion selective polymer coated electrodes through the procedures detailed below and extending its application for the selective removal of monovalent multivalent cations/anions as opposed to conventional desalination processes which do not have any selectivity. One or more embodiments may be

directed to an approach that utilizes water-soluble polyvinyl alcohol (PVA) along with crosslinkers as binders, as well as ion selective polymer coatings for MCDI electrodes. Additionally, both the electrodes as well as coatings may be deposited using simple and scalable flow coating methods.

The devices prepared in accordance with one or more embodiments herein may be fabricated to selectively remove monovalent as well as multi-valent ions from an aqueous sample that contains a blend of monovalent and divalent ions. The selective removal of monovalent and multivalent ions may be more cost-effective compared with full de-ionization that removes the most undesirable contaminants in water, including potential scalants, foulants, and precipitants for downstream processes

In one or more embodiments electrodes may be prepared by depositing an aqueous slurry of activated carbon, water soluble crosslinker, and a crosslinkable polymer on a flat substrate. One example, as shown in FIG. 3, shows a flow coating setup and flow coating mechanism. Cation and anion selectivity may be achieved by modifying the as prepared cathode and anode respectively.

One or more embodiments herein further relate to CDI device configurations that include flow-by, flow-through, flow, faradaic, inverse-, hybrid, and intercalating CDI structures both with and without membranes.

Aqueous Slurry

In one or more embodiments, a method of forming an electrode for capacitive deionization may include depositing an aqueous slurry onto a substrate, wherein the aqueous slurry comprises a porous material, a first crosslinkable hydrophilic polymer, and a crosslinker for the first crosslinkable hydrophilic polymer. In one or more embodiments, a method of forming an electrode for capacitive deionization may include annealing the aqueous slurry deposited on the substrate to create a crosslinked porous layer on the substrate.

In one or more embodiments, each component of the aqueous slurry may be included in an amount from 0.1 to 100% by weight. In one or more embodiments, on a solids weight percent basis, the porous material may be in the range of 80 to 95 wt % and the hydrophilic polymer plus crosslinker may be in the range of 0.1 to 50 wt %, or more specifically 5 to 20 wt %. In one or more embodiments, the crosslinker for the first cross-linkable hydrophilic polymer may amount from 0 to 100 mol % with respect to the moles of cross-linkable groups on the first cross-linkable polymer.

Aqueous Solution

In one or more embodiments, a method of forming an electrode for capacitive deionization may include depositing an aqueous solution comprising an ion-exchange polymer, a second crosslinkable hydrophilic polymer, and a crosslinker for the second crosslinkable hydrophilic polymer onto the crosslinked porous layer. After deposition, the aqueous solution may be annealed or dried to create a crosslinked coating layer or to otherwise provide mechanical robustness to the coating layer.

In one or more embodiments, the aqueous solution may include a blend of ion exchange polymer with the second crosslinkable hydrophilic polymer and crosslinker or the second crosslinkable hydrophilic polymer may be chemically functionalized with the ion exchange polymer. In embodiments where the second crosslinkable hydrophilic polymer is chemically functionalized with the ion exchange polymer, the functionalization may take place prior to or after depositing the aqueous solution onto the already deposited crosslinked porous layer.

Porous Material

In one or more embodiments, the porous material is selected from the group consisting of carbonaceous materials, metal organic framework, hexacyanoferrates, carbonized biomaterials, and mixtures thereof. In one or more embodiments, the carbonaceous material may be at least one of activated carbon, activated carbon fibers, aerogels, carbon nanomaterials and their composites, and monolithic carbon materials.

In one or more embodiments, ESM, or carbonized ESM may be effectively used to selectively target anionic species in a solution through electrostatic interactions and/or hydrogen bonding. More specifically, ESM may be particularly effective for adsorbing anions such as $NO3^-$ relative to other anionic species in complex solutions.

Cross-Linkable Polymer

In one or more embodiments, the first and second cross-linkable hydrophilic polymer may be, independent from each other, selected from the group consisting of polyvinyl alcohol, polyacrylic acid, crown ether, polymethylmethacrylate, glycidylmethacrylate, partially sulfonated polystyrene polymers, polyamide, polyacrylamide, chitosan, or mixtures thereof. The first and second cross-linkable polymers may be homopolymers, random co-polymers, or block co-polymers. In one or more embodiments, the first and second cross-linkable polymers may be, independent from each other, charged or uncharged. In one or more embodiments, when anion selective electrodes are desired the cross-linkable hydrophilic polymer may be quaternized polyvinyl alcohol. In another embodiment, when cation selective electrodes may be desired, polystyrene sulfonate and/or poly(3,4-ethylenedioxythiophene) (PEDOT:PSS) may be employed as a cross-linkable polymer for selectively targeting cations. The cross-linkable hydrophilic polymer may be incorporated into the second layer of the apparatus in accordance with one or more embodiments presented herein. In one or more embodiments the second layer may also include layered double hydroxides.

In yet another embodiment, a crown ether may prepared either alone or in combination with an additional hydrophilic polymer as a cross-linkable polymer for selectively targeting cations such as lithium. A specific examples of a potential lithium ionophore that may be incorporated within a cross-linkable polymer includes, but is not limited to, 2-hydroxymethyl-12-crown-4.

In embodiments where the second cross-linkable hydrophilic polymer is chemically functionalized with the ion exchange polymer, the degree of functionalization may be from 0 to 100% (i.e. from no functionalization to 100% functionalization of the second cross-linkable hydrophilic polymer).

Cross-Linker

In one or more embodiments, the cross-linker for the first and second cross-linkable hydrophilic polymers may be, independent from each other, at least one of sulfosuccinicacid, formaldehyde, glyoxal, adipic aldehyde, a dicarboxylic acid, a tricarboxylic acid, a polycarboxlic acid, anhydrides, acid chlorides, a silane, 3-glycidyloxypropyl) trimethoxysilane (GOPS), polyethylene glycol (PEG) and glutaraldehyde.

In one or more embodiments, the crosslinker for the second cross-linkable hydrophilic polymer can amount from 0 to 100 mol % with respect to the moles of cross-linkable groups on the second cross-linkable polymer. In a more specific embodiment, the crosslinker for the second cross-linkable hydrophilic polymer may be up to 30 mol % with respect to the moles of cross-linkable groups on the second

cross-linkable polymer. In one or more embodiments, the ion exchange polymer may be 0 to 20 mol % relative to the second cross-linkable hydrophilic polymer and the cross-linker for the second cross-linkable hydrophilic polymer may also be 0 to 20 mol % relative to the second cross-linkable hydrophilic polymer.

Ion-Exchange Material

In one or more embodiments, the ion-exchange material is an anion exchange polymer or a cation exchange polymer. The ion-exchange material may be dissolved into the aqueous solution prior to deposition or it may be dispersed in particulate form within the aqueous solution prior to deposition. The ion-exchange material may also be pulverized or milled before being mixed with the aqueous solution prior to deposition. In one or more embodiments, the ion-exchange material may include mono-functional or bi-functional ion-exchange groups. For example, the mono-functional ion-exchange groups may include $-SO_3H$, $-COOH$, $-PO_3H_2$, $-HPO_2H$; $-NH_3$, $-NH_2R$, $-NHR_2$, $-NR_3$. The bi-functional ion-exchange groups may include, for example, aminophosphonic acid groups, iminodiacetate groups, or variations thereof. In one or more embodiments, the ion-exchange material may be the same as the porous material. For example, a layered double hydroxide, metallic organic framework, or hexacyanoferrate may also function as an ion-exchange material.

In one or more embodiments, a particulate ion-exchange material may be processed either mechanically, chemically, or electronically to create nanosized particles or a structure to obtain greater surface area. In one or more embodiments, the processing may be at least one selected from grinding, sonicating, sieving, reduction-oxidation reactions, precipitation reactions, galvanizing, etc. In a more specific embodiment, the ion-exchange particulates may be formed by cryo-grinding the material. In one or more embodiments, the particulate material may be nanoparticles (i.e., particle average diameter between 0.1-200 nm), which may be substantially monodisperse. The average particle diameter may range from any of 0.1, 1, 5, 10, and 20 nm, to a maximum of 50, 100, 150, 200, and 500 nm. The specific ion-exchange material used may be selected to target a specific ion type (e.g., chemistry, charge, etc.).

In one or more embodiments, whether blended with or functionalized onto the second cross-linkable hydrophilic polymer, the ion exchange polymer may be from 10 to 90 wt % or from 30 to 70 wt % of the total weight of the ion exchange polymer plus the second cross-linkable hydrophilic polymer, while the second cross-linkable hydrophilic polymer may be from 90 to 10 wt % or from 70 to 30 wt % of the total weight of the ion exchange polymer plus the second cross-linkable hydrophilic polymer.

Method of Forming an Electrode

In one or more embodiments, a method of forming an electrode for capacitive deionization may include depositing an aqueous slurry onto a substrate, wherein the aqueous slurry comprises a porous material, a first cross-linkable hydrophilic polymer, and a crosslinker for the first cross-linkable hydrophilic polymer. In one or more embodiments, a method of forming an electrode for capacitive deionization may include annealing the aqueous slurry deposited on the substrate to create a crosslinked porous layer on the substrate. One or more embodiments may also separately incorporate an additional ion-exchange membrane between the cross-linked porous layer on the substrate and the feed solution containing the targeted ions.

One or more embodiments herein relate to a fabrication process that is scalable and involves the deposition of

multi-layer coatings based on cross-linkable polymers. As disclosed herein, the composition of the electrode and binder can be varied to increase electrode capacity, target specific ions, and improved energy efficiency. Additionally, the fabrication techniques disclosed herein do not require organic solvents in the fabrication of the device.

Deionizing an Aqueous Fluid

In one or more embodiments, a method of deionizing an aqueous fluid may include: continuously flowing the aqueous fluid through a capacitive deionization reactor that includes at least one electrode fabricated as described above, while applying a voltage between an anode and a cathode of the capacitive deionization reactor. In one or more embodiments, the applied voltage may be at most 2 V or at most 1.5 V. In one or more embodiments, the anode and cathode of the deionization reactor may be regenerated by reversing the sign of the applied voltage. For example, if a voltage of 1.5 V is applied to deionize an aqueous fluid then in order to regenerate the electrodes a voltage of −1.5 V may be applied so that the collected ions may be released and the electrodes regenerated. However, the regeneration voltage does not need to be an exact opposite (i.e., 1.5 V/−1.5 V), but may just be opposite in sign than the voltage applied to collect the ions on the electrode(s).

Regeneration of Electrodes

In one or more embodiments the cathode and anode may be regenerated by applying the voltage in the range of zero to the negative of the adsorption voltage value. (i.e. if applied voltage in the adsorption stage is 1.2 V then in the regeneration stage it can be any value between 0 and −1.2 V). For some electrode materials, a negative voltage of lower than 1.2 V can also be utilized to enhance desorption performance.

EXAMPLES

In accordance with one or more embodiments of the invention, the Examples noted below detail the use of electrodes within CDI and MCDI systems wherein the electrodes are fabricated to selectively and preferentially target and remove single or multivalent ions through capacitive deionization.

Examples of Electrode Preparation

Example 1 PVA-GA Electrode

In accordance with one or more embodiments herein, electrodes may be fabricated and coated with ion-exchange polymers wherein the porous electrodes may be fabricated to specifically and selectively remove ionic species from aqueous solutions. In one or embodiments the composition of a porous electrode may consist of 90 wt % high-surface-area powdered activated carbon (PAC) and 10 wt % of the polymeric binder (linear polymer PVA and cross-linker GA) based on the total mass of dry electrodes.

In one embodiment the fabrication of a porous electrode may involve three main steps: slurry preparation, casting, and drying/annealing. In an example, first, a 6 wt % PVA solution was prepared by mixing a desired amount of PVA in DI water at 90° C. for 4 h. Next, a glutaraldehyde (GA) solution (5 mol % relative to PVA repeat units) was added and mixed for 1 hour. PAC was added slowly along with additional DI water, giving the final solid content of the slurry of approximately 30 wt %. The resulting mixture was stirred for 12 h to ensure homogeneity. Next, the homogeneous carbon slurry was deposited directly onto graphite sheets through slurry casting with a gap height of 300 μm.

The graphite sheets served as current collectors and were rinsed with DI water first and then adhered to a glass plate using polyimide tape. After slurry deposition, electrodes were dried in air and annealed at 130° C.

Example 2 PVDF Electrode (For Comparison)

PVDF bound electrodes are more commonly used in commercial CDI reactors. For the purpose of comparison, a PVDF was prepared as follows. First, PVDF was dissolved in DMAc (4 wt % solution) for 1 h followed by an addition of activated carbon (90 wt % of the total dry mass). The resulting mixture (approximately 30 wt % solid) was continuously stirred for 12 h. The homogeneous slurry was deposited on a graphite sheet using the slurry casting method with a gap height of 250 μm and dried in the oven at 60° C. for 2 h followed by overnight vacuum drying for complete solvent removal. Prior work has shown that the different mass (or carbon content) and thickness of the electrodes can lead to a different degree of electrode utilizations for similar operating conditions. In this work, the gap height was chosen to produce a similar final electrode mass and thickness comparable to that of PVA-bound electrodes.

Ion Selective Electrode Formation Examples

In accordance with one or more embodiments herein, ion-selective electrodes may include composite electrodes (comprised of porous active material held together by a polymeric binder) that provide selective permeability to multivalent ions. While similar devices have been discussed and reported, the presently described designs are the first practical and effective realization of this type of device. It is been demonstrated herein that specific chemistries may be incorporated to enable selective uptake of multi-valent ions. These chemistries can be tailored to target specific contaminants.

Cation Selective Electrodes

Example C1

A commercial ion-exchange resin (for example, but not limited to, Dow chemical, Amerlite IRC747) was cryo-grinded with liquid nitrogen to achieve the smallest particle. Before coating, particles were sonicated using Ultracell Sonicator VCX-500. To form an ion-exchange polymer (ISP) layer, the particles were mixed with PVA, SSA, and GA and flow coated on the carbon electrode with total weight ratio of 54.2:40.8:4.1:0.9 (particle: PVA:SSA:GA). The mixed slurry may be coated on top of any kind of carbon electrode using the flow coating method. In this Example, the porous electrode of Example 1 was coated as described above before the coated electrode was then cross-linked in a vacuum oven carefully maintained at 80° C. for 12 hours. Cross-linking temperature may be narrowly controlled, as at lower temperatures the PVA/SSA/GA mixture may not sufficiently cross-link which can result in deformation of the PVA layer. On the other hand, at higher temperatures, crosslinked polystyrene resin particles may be damaged. Therefore, it is important to maintain the optimum conditions (formula, coating speed, coating depth, temperature, and reaction time) for fabricating a homogeneous and dense hydrogel ion exchange layer. The surface morphologies of the uncoated carbon and the ISP composite electrodes were examined by scanning electron microscopy (SEM, FEI Quanta 400).

Example C2

In this example, prepared in similar fashion to cation exchange layer described in Example C1, the porous cath-

ode of Example 1 was first coated with PVA+SSA/GA aqueous mixture and then modified with iminodiacetic acid (IDA) as shown in FIG. **4**.

Example C3

The cation-exchange polymer coating was comprised of poly(vinyl alcohol) (PVA) and sulfosuccinic acid (SSA) and was synthesized by adapting procedures reported in the literature. A 6 wt % PVA solution was prepared in DI water, and SSA (20 wt % relative to PVA weight) was added followed by mixing for 1 h at room temperature to ensure homogeneity. The resulting mixture was deposited onto the electrode prepared in Example 1 (with PVA binder) and cross-linked by annealing at 130° C. The cation exchange polymer coated electrode was used as the cathode in the MCDI cell system as depicted in FIG. **5**.

Example C4

A Ca^{2+} selective nanocomposite (CSN) electrode was prepared by casting a nanocomposite coating containing Ca^{2+} selective ion exchange nanoparticles on the surface of the carbon electrode. A top-down approach was used to first obtain nano-sized Ca^{2+} selective ion exchange resin particles. To obtain nanoparticles without altering their surface chemistry, an Amberlite™ IRC747 resin was cryo-ground using a freezer mill with a milling program consisting 5 cycles of alternating grinding (2 min) and cooling (1 min). The resin nanoparticles were then sonicated in liquid nitrogen for 1 min and then mixed with PVA (6 wt %), GA (25 wt %), and SSA (75 wt %) solutions at a dry weight ratio of 54.2:40.8:4.1:0.9 (resin nanoparticle: PVA:GA:SSA). The slurry was then cast on the preformed carbon electrode, as described in Example 1, using the flow coater at 1 mm/s with a casting slit width of 30 mm. Finally, the coated electrode was dried at room temperature for 12 h and the binder was cross-linked in a vacuum oven at 80° C. for 12 h. All electrodes were precisely cut into 1 cm×10 cm coupons before used in the electro-sorption device.

Example C5

A Ca^{2+} and Ba^{2+} selective electrode was prepared by coating the surface of the carbon electrode of Example 1 with a mixture of PEDOT:PSS (1.3 wt % in D.I. water) crosslinked with GOPS (0.6 vol % of total PEDOT:PSS solution). An example of such a fabricated electrode is provided in FIG. **25**.

Anion Selective Electrodes

Example A1

Similar to the Example C1, a commercial anion exchange resin was crushed into fine powder to produce anion exchange nanoparticles, prior to being mixed with a quarternized polyvinyl alcohol (QPVA)+GA mixture. The resulting mixture was then flow coated onto the anode comprising the porous electrode of Example 1, shown in FIG. **6**. A resin coated carbon electrode with a size of 5 cm×10 cm was utilized in a CDI to evaluate the selectivity of sulfate over chloride.

Example A2

Similar to Example A1 the anion-exchange polymer coating was composed of quaternized poly(vinyl alcohol)

(QPVA) cross-linked with GA and was synthesized in similar fashion. Specifically, KOH (50 mol % relative to PVA repeat units) and glycidyl trimethylammonium chloride (GTMAC, 50 mol % relative to PVA repeat units) were added to a 6 wt % PVA solution in DI water. Next, the mixture was heated at 70° C. for 4 h while stirring continuously. After cooling to room temperature, the resulting mixture was precipitated in pure ethanol and dried overnight under vacuum to obtain QPVA as a white solid. This product was dissolved in deionized water at 90° C., and the pH was lowered to 5 by adding 1.0 M HCl solution. To this solution, GA cross-linker (10 wt % relative to PVA) was added and stirred for 1 h. The resulting mixture was deposited onto the surface of the electrode as prepared in Example C1 (with PVA binder) and cross-linked at 130° C. for 1 h. The anion-exchange polymer-coated electrode was used as the anode in the MCDI system of FIG. **5**.

Example A3

The sulfate selective electrodes were fabricated by casting a layer of QPVA containing pulverized AMBERLITE FPA54 resin onto the carbon electrode, as prepared in Example 1, before the electrode was heated for cross-linking. To prepare the resin slurry, batches of 0.5 g AMBERLITE FPA54 resin were pulverized by cryogenic milling (6750 FREEZER/MILL, SPEX SamplePrep, U.S.A.). The milling program consisted of 15 min cooling in liquid nitrogen, followed by 5 cycles of alternating grinding (2 min) and cooling (1 min), and was repeated once for every batch of resin. The resin powder was then sieved with a 50 μm stainless-steel mesh and mixed with 6 wt % QPVA and GA with a resin-to-QPVA weight ratio of 1:1 and 4.4 mol % glutaraldehyde relative to QPVA repeating units. After homogenization, the resin/QPVA slurry was flow-coated on the air-dried carbon electrode at a loading of 0.03 mL slurry/cm²-electrode unless otherwise specified, and heated overnight in a vacuum oven at 70° C. for cross-linking.

Example A4

Example A4 served as a control electrode for Example A3 and was fabricated using an identical protocol. All electrodes were stored in DI water, and conditioned in the corresponding feed solution (1.0 L) for at least 1 day before each experiment.

Selective Ion Removal Experiments

Study 1 Evaluation of Ion-Exchange Coated Porous Electrodes

Desalination tests were conducted using both PVA- and poly PVDF-bound electrodes as prepared with electrodes of Examples 1 and 2, in addition to electrodes coated with ion-exchange coatings, such as Examples C3 and A2 (PC-MCDI), or using bare electrodes (Example 1) along with commercial ion-exchange membranes (MCDI). PVA and PVDF bound electrodes were prepared in accordance with Examples 1 and 2 above, respectively, and are of identical size (10 cm×1 cm) and similar total mass for comparison. Below, the performance of PVA-CDI (Example 1) and PVDF-CDI (Example 2) systems was first compared, followed by an analysis of the PVA-PC-MCDI (Example C3) system with the ion-exchange polymer coatings and PVA-MCDI (Example 1 with commercial ion-exchange membrane) and PVDF-MCDI (Example 2 with commercial ion-exchange membrane) systems that contain commercial ion exchange membranes.

Deionization tests were conducted in order to evaluate the selective ion removal performance of the prepared electrodes described in Examples 1, 2, C1, C2, and Example A1. In FIG. 7, a lab scale deionization set up is shown. A pair of ion selective polymer coated electrodes prepared in accordance with the Examples referenced above were inserted into a flow-by CDI cell with a pair of ion exchange membranes and tested with the mixture of the monovalent and divalent ion feed solution. During operation, the CDI effluent was continuously measured in terms of conductivity and ion species. Later, the ions in the product water were precisely analyzed by either ICP-OES or IC. Mixed salt solutions containing two different concentrations (5 mM NaCl and 5 mM Na_2SO_4 (1:1), 50 mM NaCl and 5 mM Na_2SO_4 (10:1)) were utilized in this study. The flow rate was 0.5 mL/min. The adsorption and desorption voltage were 0.4 V and 0 V respectively. The adsorption/desorption cycle was 30 min.

To evaluate selective removal of multi-valent cation/anions over mono-valent cation/anions, respectively, a selectivity performance index (SPI, Formula (1)) has been developed. The ratio of accumulated amount of adsorbed ions is divided by a constant initial (feed) concentration ratio value. The selectivity performance index gives us a representative number to compare selective ion removal for a wide range of feed concentrations and mono/di-valent ion ratios.

$$SPI = \frac{\sum Conc\_Multi_{abs}}{\sum Conc\_Mono_{abs}} \bigg/ \frac{Conc\_Multi_0}{Conc\_Mono_0} = \frac{\sum Ca_{abs}}{\sum Na_{abs}} \bigg/ \frac{Ca_0}{Na_0}$$

For example, the calcium ion selectivity over sodium in this specific Experiment for Example C1 was calculated using the same approach. With different mixing (molar) ratios (Na to Ca, 1:1, 2:1, 4:1, and 10:1, respectively), initial Ca/Na-SPI is equal to one, which means the same amount of both the ions were removed. SPI changes with respect to time and different mixture ratios and is shown in FIG. 8. As shown in FIG. 8, the Ca/Na SPIs at the outset were almost the same and were observed to gradually increase. After a certain period of charging time (after 15 min in this case), the SPI of the lower mixing ratio (2:1) increased much more rapidly than that of the higher mixing ratio. The final SPI at 30 min for 2:1 (11.6) was recorded as the highest Ca-specific selectivity, as shown in Table 1.

TABLE 1

Ion selectivity for different feed concentrations and mixing ratios for a coated electrode of Example C1.

	ΣCa	ΣNa	Selectivity
2:1	20.2 μM (808 μg)	3.5 μM (80 μg)	11.6
4:1	17.4 μM (696 μg)	24.0 μM (552 μg)	2.90
10:1	11.8 μM (471 μg)	48.9 μM (1,124 μg)	2.41

Similarly, for Example C2, results are shown for the electrodes just coated with PVA+SSA mixture (Example C1) and two other samples of Example C2 (C2A and C2B) modified with IDA as described above. In this approach, all the experiments were conducted using feed solution of 1:1 Ca/Na molar ratio with the total concentration of 10 mm. Electrodes with only PVA+SSA coating provided the selectivity ratio of 0.9, approximately. The electrodes of Example C2 with IDA modification showed significant improvement

in selectivity, as demonstrated in FIG. 9. This indicates that a wide range of selectivity values from 1.5 to 4.59 can be obtained in different conditions. With careful optimization of the coating layer and the IDA modification procedure a very high selectivity can be obtained.

As shown in FIGS. 10A-10C, for Example A1 the removal efficiency of SO_4^{2-} during adsorption period was much higher than Cl^-, indicating that the resin coated CDI has selectivity for SO_4^{2-} over Cl^- at a Cl^-/SO_4^{2-} concentration of 5:5 (FIG. 10A), which was about 2.0 during adsorption period (FIG. 10C). When the Cl^- concentration increased 10 times to a Cl^-/SO_4^{2-} concentration of 50:5 (FIG. 10B), the removal behavior of SO_4^{2-} illustrated little change (despite that the removed Cl^- increased), indicating that the resin coated CDI has great selectivity of SO_4^{2-} over Cl— even at higher Cl^-/SO_4^{2-} ratios (FIG. 10C). The selectivity of SO_4^{2-} over Cl^- at Cl^-/SO_4^{2-} concentration of 50:5 ranged from 2.1 to 2.8 during adsorption period (FIG. 10C).

Study 2-Analysis of Ion-Exchange Coating on Porous Electrode

In this study, a "flow-by type" CDI unit cell was fabricated and assembled into a lab-scale setup, as shown in FIG. 7. The setup included feed solution tank, a peristaltic pump (Cole-Parmer Masterflex, feed pressure <20 kPa), a CDI cell assembly (FIG. 5), an electrochemical analyzer for power supply, and in-line pH and conductivity meters at the exit of the CDI cell and effluent collection tank. The CDI assembly included two electrodes, cation/anion exchange membranes, and graphite current collectors. The two sides of the assembly were separated by a 1-mm-thick woven nonconductive nylon spacer (61% porosity). Additionally, a computer system interfaced with the electrochemical analyzer and the pH and conductivity meters to automatically log the electrical current, pH, and conductivity data, respectively. Current and conductivity values were recorded at 1-s intervals. The pH values were recorded at 10-s intervals and linearly interpolated to estimate the pH for 1-s intervals. Changes in the effluent pH are common for both CDI and MCDI systems and reflect a combination of Faradaic reactions and migration of H^+ and OH^- ions to the electrodes. The contributions of H^+ and OH^- ions to the measured effluent conductivity were accounted for based on the standard molar conductivities for each ion: 329.82 and 198.6 mS L mol^{-1} cm^{-1} for H^+ and OH^-, respectively. The molar concentrations of H^+ and OH^- were calculated based on the effluent pH, and the conductivity contribution of H^+ and OH^- ions was then subtracted from the measured effluent conductivity value to give corrected conductivity values. The corrected conductivity values were then converted to NaCl concentration (mg/L) using feed solution conductivity-concentration relationship (10 mM NaCl, 1.130 mS/cm).

The salt removal performance of the electrodes was evaluated using 10 mM NaCl feed solution and 10 cm×1 cm electrode size (10 cm^2 electrode cross-sectional area). Prior to testing, the electrode assembly was equilibrated by running the feed solution continuously for 1 h with no voltage bias. During testing, a constant DC voltage was cycled on (1.2 V) and off (0.0 V) at intervals of 1000 s (16.67 min). The performance of the different types of systems was quantified in terms of the salt adsorption capacity (SAC), average salt adsorption rate (ASAR), salt removal efficiency (SRE), and charge efficiency (CE).

The salt adsorption capacity (SAC, Formula (2)) represents the total salt removed during one adsorption cycle normalized by the total electrode weight. The electrode weight $W_{electrode}$ is the combined weight of both electrodes

including the activated carbon and polymeric binder but excluding the ion-exchange polymer layer or ion-exchange membrane:

$$SAC = \frac{Q^* \int (C_o - C_t) dt}{W_{electrode}}$$ Formula (2)

Where Q is the volumetric flow rate of the solution, and C_o and C_t are the feed and effluent NaCl concentrations (mg/L) respectively. The feed concentration C_o is constant during desalination.

The average salt adsorption rate (ASAR, Formula (3)) is calculated by dividing the SAC by the duration of the adsorption cycle (t_{cycle}=1000 s):

$$ASAR = \frac{SAC}{t_{cycle}}$$ Formula (3)

The salt removal efficiency (SRE, Formula (4)) represents the fraction of salt removed per adsorption cycle normalized by the inlet salt concentration:

$$SRE = \frac{\left(\int (C_o - C_t) dt \right)}{(C_o^* t_{cycle})}$$ Formula (4)

The charge efficiency (CE, Formula (5)) is the ratio of moles of salt removed relative to the charge supplied during the adsorption step where m is the molecular weight of NaCl (58.44 g/mol) and F is Faraday's constant, 96 485 C/eq.

$$CE = \frac{\left(Q^* \int (C_o - C_t) dt / m \right)}{(\int I^* dt / F)}$$ Formula (5)

Desalination tests were conducted using both PVA and poly PVDF-bound electrodes, Examples 1 and 2, and either using bare electrodes (CDI), electrodes coated with ion-exchange coatings, Examples C3 and A2 (PC-MCDI), or using bare electrodes along with commercial ion-exchange membranes (MCDI). PVA and PVDF bound electrodes were prepared in accordance with Examples 1 and 2 above, respectively, and are of identical size (10 cm×1 cm) and similar total mass for comparison. The coatings and electrodes were stable when immersed in water during desalination tests. Below, the performance of PVA-CDI and PVDF-CDI systems was first compared, followed by an analysis of the PVA-PC-MCDI system with the ion-exchange polymer coatings and PVA-MCDI and PVDF-MCDI systems that contain commercial ion exchange membranes. The performance parameter values reported herein were for the average of 5 cycles of the same sample.

Detailed studies on repeatability were not carried out, but in general, there was a variation of 5% in performance for electrodes fabricated using the same processing conditions and composition. Desalination tests were conducted to understand the effect of binder on the salt removal performance and charge efficiency.

Comparison of Porous Electrode of Example 1 and Example 2

Porous Electrodes of Examples 1 and 2 are compared in FIG. 11A wherein the effluent conductivity for both systems are shown over 5 cycles of operation. During the adsorption cycle on the application of a constant voltage (1.2 V), the effluent conductivity decreases sharply and then increases over time as the electrodes saturate. During the desorption cycle (0.0 V), the effluent conductivity rises sharply and then again decreases as it returns to the feed conductivity. Effluent conductivity for one adsorption/desorption cycle shown in FIG. 11B indicates the presence of the small inverted peak at the beginning of adsorption cycle for the Example 1 system. This has been reported previously and is known as the "inversion effect" and is attributed to co-ion expulsion from the electrodes. This inversion effect leads to reduced salt removal and charge efficiency. It is unclear why an inversion effect is observed for PVDF-bound electrodes of Example 2 only, but this may indicate lower co-ion adsorption for the Example 2 system.

As presented in FIG. 11C, the electrode of Example 1 has a 41% higher salt adsorption capacity (SAC) and average salt adsorption rate (ASAR) relative to PVDF-CDI system. Similarly, the salt removal efficiency (SRE) and charge efficiency (FIG. 11D) is 48% and 59% higher for the system comprising the electrodes of Example 1. This performance difference may be attributed in part, to the minimized inversion effect in the electrode of the system of Example 1 as compared to Example 2 electrode system. Cyclic voltammetry measurements show a much higher specific capacitance for the PVA-bound electrodes compared with PVDF-bound electrodes. Furthermore, as demonstrated through water contact angle analysis PVA bound electrodes are more hydrophilic, which may lead to enhanced ion uptake.

These studies demonstrate that, in addition to the straightforward and scalable fabrication procedures without the use of the organic solvents, the uncoated PVA-CDI system may produce superior results to PVDF electrodes in terms of salt removal performance and charge efficiency.

Comparison of Electrodes in Example 1 and Example C3

Analysis of the effluent conductivity (FIGS. 12A-12B) revealed a larger salt uptake in the case of Example C3. Averaged over 5 cycles, the amount of salt removed per adsorption cycle was 1.74 mg (29.8 μmol) and 2.66 mg (45.5 μmol) for the Example 1 system and Example C3 system, respectively. Furthermore, the SAC and ASAR (FIG. 12C) were both higher for the Example C3 system by approximately 57%, and the SRE and charge efficiency (FIG. 12D) were improved by 53% and 51%, respectively, for the PVA-PC-MCDI system relative to PVA-CDI system. This performance enhancement may be attributed to the presence of the ion-exchange polymer coatings. The ion-exchange polymer coatings block co-ions from penetrating the electrodes and give increased salt adsorption capacity and charge efficiency. Notably, the salt adsorption capacity of the coated PVA-bound electrodes is higher than typically reported (5-13 mg/g) in the literature for other activated-carbon-based electrodes. This may be attributed to a combination of improved wettability of the electrodes due to hydrophilic polymer binder, the high surface area of activated carbon, and the presence of the ion-exchange polymer coating.

Analysis of the effluent conductivity and effluent pH over a 24-h experiment suggest that the ion-exchange polymer coatings significantly reduce the occurrence of Faradaic reactions, and hence improve stability and long-term performance.

Comparison of Example 1, Example 2, and Example C3 in MCDI Reactors

A variety of ion-exchange membranes are available commercially, and a common approach to fabricate MCDI systems is to place commercial ion-exchange membranes on top of porous electrodes. Commercial ion-exchange membranes are typically as thick as the electrodes (250-300 μm), resulting in significantly increased module size and weight. The thickness of commercial ion-exchange membranes used in this work is 450-μm thick, roughly 45 times the thickness (about 10 μm) of the ion-exchange polymer coating used in these experiments. To evaluate the effectiveness of the ion-exchange polymer coating, a PVA-PC-MCDI (Example C3 within MCDI system) system was compared to a similar PVA-MCDI system with PVA-bound electrodes, in accordance with Example 1, and commercial ion-exchange membranes. In addition, the performance of the PVA-PC-MCDI system was compared to that of PVDF-MCDI (Example 2 within MCDI system), which included commercial ion exchange membranes on top of PVDF-bound electrodes.

Analysis of the effluent conductivity over 5 cycles of operation, presented in FIG. 13A, indicates reversible electro-sorption for all the three systems. Careful analysis of one adsorption/desorption cycle (FIG. 13B) indicates a higher initial salt uptake rate for the PVA-PC-MCDI system as compared to the other two systems. This suggests that the thin (10 μm) ion-exchange polymer coating layer may have lower area resistance (<2.0 Ωcm^2) and therefore higher initial salt uptake rates compared to the thick (450 μm) commercial ion-exchange membranes (electrical resistance approximately 30 Ωcm^2).

Furthermore, the quantitative comparison of salt removal performance presented in FIG. 13C and FIG. 13D indicates that the PVA-PC-MCDI system has a reduced SAC, ASAR, SRE, and charge efficiency when compared with the PVA-MCDI system. This reduced performance (salt removal and charge efficiency) may be attributed to ion leakage through the thin ion-exchange coatings, resulting in co-ion adsorption in the PVA-PC-MCDI system. To improve the performance of the PVA-PC-MCDI electrodes, optimization of coating layer thickness, composition (charge and cross-linking density), and uniformity may be used.

The effluent conductivity and effluent pH indicate a very stable performance for all three systems. This suggests little or no Faradaic in MCDI systems. In summary, a simple and scalable aqueous based approach was demonstrated for the preparation of electrodes using activated carbon and water-soluble PVA binder without the use of organic solvents. The as-fabricated electrodes were further coated with aqueous solutions of sulfonated (cation exchange) and aminated (anion exchange) polymers to produce the MCDI system. Desalination tests for the polymer-coated electrodes exhibit salt adsorption capacities up to 14.4 mg/g and charge efficiencies up to 86.3%. Furthermore, PVA binder-based electrodes exhibited an adsorption capacity and charge efficiency of 16.1 mg/g and 97.1%, respectively, when paired with commercial ion-exchange membranes. PVA bound electrodes exhibited salt uptake capacities exceeding 18.0 mg/g when paired with low-resistance commercial ion-exchange membranes. Notably, the obtained salt adsorption

capacities and charge efficiencies are higher than typically achieved for activated carbon electrodes with a hydrophobic polymer binder.

Study 3 Selective Sulfate Removal Study

CDI experiments were performed using the uncoated, QPVA coated (Example A4), or resin/QPVA coated (Example A3) electrodes as the anode, and an uncoated carbon electrode with a CEM as the cathode. All experiments were performed in the flow-by (i.e., single pass) mode for at least 12 h (FIG. 14). During operation, binary solutions containing different concentrations of NaCl and Na_2SO_4 were continuously pumped into the CDI reactor at 1.0 mL/min for all experiments. The adsorption and desorption cycles were set at 1.5 h unless otherwise specified. The applied voltage was 1.2 V during adsorption and 0 V during desorption. A multistep potential method was utilized to provide constant voltage using a potentiostat, and the current was recorded by the potentiostat at 1 s intervals. Effluent conductivity was recorded at 1 s intervals using a micro conductivity meter. Both the potentiostat and the micro conductivity meter were interfaced with a computer for continuous automatic recording of data (FIG. 14). Effluent samples were also collected at 2 min intervals for analysis of SO_4^{2-} and Cl^- concentrations by ion chromatography. An uncoated electrode (5×1 cm2) was used as the counter electrode.

The carbon electrodes in each sample of this experiment were prepared in similar fashion to Example 1.

FIGS. 15A-15C show SEM images of the surface and cross-section of the pristine activated carbon electrodes. The PAC particle size ranged between 1 and 10 μm, and the electrodes were approximately 300 μm thick. Casting 0.03 mL/cm^2 resin slurry on the carbon electrode resulted in a ~23 μm thick composite film on the carbon electrode surface (FIGS. 15D-15E). The resin powders blended uniformly with the QPVA binder. In contrast, the QPVA coated electrode has a dense and homogeneous polymeric coating, with a thickness of ~10 μm.

FTIR analysis (FIG. 15F) of the carbon electrode showed two small peaks at 2914 and 2850 cm^{-1}, corresponding to C—H and CH2 stretches, respectively. This confirms the presence of the PVA binder in the carbon electrode. The QPVA coated carbon electrode of Example A4 showed strong C—H, C—O, N—H and amide III stretches, consistent with its molecule structure. The spectrum of the resin powder contained amide I and N—H stretches but relatively lower C—H stretches compared with QPVA. The spectrum of the resin/QPVA electrode of Example A3 exhibited features of both the resin powder and QPVA with stretches corresponding to nitrogen functional groups that can provide affinity for divalent anions (such as sulfate) over monovalent ions. EIS showed that the uncoated electrode had an Ohmic and diffusion resistance of 16.2 and 29.7Ω, respectively, much lower than that of QPVA coated electrode (31.0 and 41.9Ω, respectively) and resin/QPVA coated electrode (22.0 and 35.0Ω, respectively).

In the CDI experiments, all electrodes produced highly reproducible current and effluent conductivity in a large number of adsorption and desorption cycles. The very high consistency between the adsorption and the desorption currents suggests that ion adsorption was completely reversible. The adsorption and desorption currents of the uncoated electrode (Example 1) was higher than those of the QPVA (Example A4) and resin/QPVA coated electrodes (Example A3), which was attribute to its lower resistance.

Desalination performance was assessed by total salt removal (SR, mequiv/m2 (Formula 6), or mg/g equivalent to NaCl adsorption (Formula 7)) and specific ion removal (IR,

mmol/m2) during an adsorption cycle per unit electrode surface area (m2) (Formula 8). Charge efficiency (CE) represents the ratio of ions removed to the number of charges supplied during the adsorption cycle as defined in Formula 9.

$$SR = \frac{Q \int_0^t \left(C_{Cl^-,inf} - C_{Cl^-,eff} + 2\left(C_{SO_4^{2-},inf} - C_{SO_4^{2-},inf} \right) \right) dt}{A_e}$$ Formula 6

$$SR = \frac{QM \int_0^t \left(C_{Cl^-,inf} - C_{Cl^-,eff} + 2\left(C_{SO_4^{2-},inf} - C_{SO_4^{2-},inf} \right) \right) dt}{m_e}$$ Formula 7

$$IR = \frac{Q \int_0^t (C_{i,inf} - C_{i,eff}) dt}{A_e}$$ Formula 8

$$CE = \frac{F \cdot Q \int_0^t \left(C_{Cl^-,inf} - C_{Cl^-,eff} + 2\left(C_{SO_4^{2-},inf} - C_{SO_4^{2-},inf} \right) \right) dt}{\int_0^t I \, dt}$$ Formula 9

Here, Q (L/s) is flow rate, $C_{Cl^-,inf}$, $C_{SO_4^{2-},inf}$, $C_{Cl^-,eff}$, and $C_{SO_4^{2-},eff}$ (mmol/L) are Cl^- and SO_4^{2-} concentrations in the influent (inf) and effluent (eff), respectively; t (s) is duration of the adsorption cycle; i is a specific ion, Cl^- or SO_4^{2-}; A_e (m^2) is the effective frontal area of anodes; M is the mole weight of NaCl (58.5 g/mol); m_e is the total mass of the two electrodes (include the PVA material but not include the graphite sheet); F is Faraday's constant (96,485 C/mol); and I is the current (A).

Selectivity ($S_{i/j}$) between two competing ions i and j is defined by Formula 10, where the numerator and denominator represent the ratio between the solid phase concentration (or amount adsorbed) and the influent concentration (i.e., equilibrium aqueous phase concentration at adsorption saturation) of ions i and j, resnectively.

$$S_{i/j} = \frac{\int_0^t Q(C_{i,inf} - C_{i,eff}) dt / C_{i,inf}}{\int_0^t Q(C_{j,inf} - C_{j,eff}) dt / C_{j,inf}}$$ Formula 10

Desalination Performance and SO_4^{2-} Selectivity

Experiments were first conducted using a bisolute solution containing 5 mmol/L NaCl and 5 mmol/L Na$_2$SO$_4$. As shown in FIG. 16A, the uncoated electrode of Example 1 achieved an adsorption capacity of 13.6±0.4 and 13.8±0.6 mmol/m^2 for SO_4^{2-} and Cl^-, respectively, with a total salt removal of 41.0±0.9 mequiv/m^2 (11.5 mg/g) and charge efficiency of 46.2%±1.0% (FIG. 16E). When coated with QPVA in Example A4, the SO_4^{2-} and Cl^- removal increased to 17.4±0.8 and 19.6±1.0 mmol/m^2 respectively. The adsorption capacity and charge efficiency increased significantly to 54.4±2.6 mequiv/m^2 (15.3 mg/g) and 86.1%±4.1% (FIG. 16E) respectively. The large increase in charge efficiency confirms that the quaternary amine functional groups on the QPVA provide anion exchange capacity and exclude cations. The total anion adsorption capacity did not increase proportionally with the charge efficiency. This may be attributed to the increase in electrode resistance when it is coated with QPVA. The QPVA coating also resulted in significantly more Cl^- adsorption than SO_4^{2-}. This may be attributed to the higher relative diffusivity of Cl^- versus SO_4^{2-} compared

to that in the bulk solution, which has been observed in electrodialysis systems. Further discussion is provided in the next section.

The resin/QPVA coated electrode of Example A3 exhibited a salt adsorption capacity of 58.4±1.4 mequiv/m^2 (16.4 mg/g, SO_4^{2-} and Cl^- removal of 23.9±0.6 and 10.6±0.9 mmol/m^2 respectively), 42% and 7% higher than that of the uncoated Example 1 electrode and the QPVA coated electrode of Example A4. Compared to both the uncoated and QPVA coated electrodes, the resin/QPVA coated electrode in Example A3 had much higher SO_4^{2-} adsorption (76% and 37% increase, respectively), and notably lower adsorption for Cl^- (23% and 46% decrease, respectively) (FIG. 16A). Example A3 exhibited significant selectivity for SO_4^{2-} over Cl^-.

As shown in FIG. 16D, the SO_4^{2-} to Cl^- selectivity as defined in Formula 5 increased from 1.37 at the beginning of the adsorption cycle to 2.24 when adsorption reached equilibrium, while the uncoated and QPVA coated electrodes of Examples 1 and A4 had SO_4^{2-} to Cl^- selectivity lower than 1. During desorption, the released amounts of SO_4^{2-} (23.7±0.4 mmol/m^2 99.2% recovery) and Cl^- (10.4±0.4 mmol/m^2 98.1% recovery) (FIG. 16C) were consistent with the adsorption selectivity observed, indicating that the selective adsorption process was completely reversible. Interestingly, the charge efficiency of the resin/QPVA coated electrode in Example A3 was 66.5%±1.6%, which was lower than that of the QPVA coated electrode, although still 44% higher than that of the uncoated electrode. It is speculated that the reduced charge efficiency compared to that of the QPVA coated electrode may be caused by imperfection at the interface of the resin particle and the QPVA matrix (FIG. 15E), which allows more co-ions (i.e., cations) to transport through. On the basis of the salt removal and current generation data, the energy consumption for SO_4^{2-} removal was 431.1 kJ/mol-of-SO_4^{2-} removed for the resin/QPVA coated electrode, significantly lower than the uncoated electrode (755.5 kJ/mol-of-SO_4^{2-} removed).

Influence of Resin Coating Thickness

Although it renders selectivity, a coating on the electrode surface may also increase ion transport resistance and hence hinder removal kinetics. To evaluate the influence of coating thickness on adsorption kinetics, the amount of resin slurry deposited was increased from 0.03 mL/cm^2 to 0.06, 0.08, and 0.1 mL/cm^2 resulting in resin/QPVA coating thicknesses of 23.1±2.1, 42.4±1.9, 48.3±4.7, and 65.7±3.0 μm for samples prepared as described in Example A3, respectively (FIGS. 17A-17E). A thin coating (slurry loading at 0.03

mL/cm2) resulted in notably greater salt removal (FIG. **18**A and FIG. **18**B). This may be attributed to the exclusion of co-ions by the coating, which increased charge efficiency from 44.7% (uncoated) to 70.8% (0.1 mL/cm2 loading of the resin/QPVA slurry, FIG. **18**C).

Further increase in coating thickness led to slight increase in salt adsorption capacity despite the slight decrease in the average electric current during the adsorption cycle. These results suggest that the additional electric resistance from the coating did not have a significant impact on the salt removal. The very small changes in adsorption capacity with thicker coatings also suggest that the resin/QPVA coating does not contribute to the adsorption of the anions. But more notably, it primarily affects the ion transport.

The thinnest coating increased the SO_4^{2-} to Cl^- selectivity from 0.96 (uncoated electrode) to 2.33, and the selectivity increased slightly with increasing coating thickness, reaching 2.57 with 0.1 mL/cm2 loading of the resin/QPVA slurry. However, thicker coatings did hinder adsorption and desorption kinetics as shown in FIG. **18**A, underlining the role of optimizing the coating thickness and composition to improve performance.

Long Term Stability of Resin/QPVA Electrode

The resin/QPVA-coated electrode was continuously operated for 50 cycles with adsorption/desorption period of 30 min to evaluate its long-term stability. As shown in FIG. **19**A, the current production and effluent conductivity exhibited excellent repeatability during the 50 h operation. Analysis of specific ion concentrations during the 2nd and 50th cycle showed almost identical evolution of ion concentrations in the effluent (FIG. **19**B).

Through the Examples provided above it was demonstrated that selective removal of SO_4^{2-} in the presence of a wide range of Cl^- concentrations may be achieved using a carbon electrode coated with a thin film containing QPVA and SO_4^{2-} selective resin. The resin/QPVA coating not only functions as an anion exchange membrane to mitigate adsorption of co-ions, but may allow preferential transport of SO_4^{2-}, resulting in significantly improved charge efficiency as well as strong selectivity for SO_4^{2-} over a wide range of Cl^-: SO_4^{2-} concentration ratios. The transport rate of anions through the resin/QPVA coating seems to be qualitatively consistent with the "solution-diffusion" model, where the solubility or partition coefficient and diffusivity of the ion determine its transport rate. Interestingly, the SO_4^{2-} selectivity only decreased slightly when the influent Cl^-: SO_4^{2-} concentration ratio increased from 1:1 to 20:1, much less than what the solution diffusion model would predict. These results suggest that the interactions between the anions and the composite resin QPVA coating are complex and heterogeneous due to the presence of microscale domain of high SO_4^{2-} affinity (i.e., the resin particles), and the nonselective matrix (i.e., QPVA).

Compared to the QPVA coating, the resin/QPVA coating slightly reduced charge efficiency, and the charge efficiency is significantly lower than that of commercial anion exchange membranes. However, this may be proved by further reducing the size of the cryo-ground anion exchange nano-sorbent resin.

Study 4 Selective Calcium Removal Study

In this study, a simple yet highly effective method to achieve calcium-selective removal in an electrosorption process by coating the cathode with a calcium selective nanocomposite (CSN) layer using an aqueous phase process is demonstrated. The carbon electrodes were prepared in accordance with Example 1. The calcium selective nanocomposite electrode was prepared as described in Example C4.

The ion removal performance of the electrodes was evaluated in flow-by the MCDI system illustrated in FIG. **20**. A bare carbon electrode was used as the anode in all experiments, and the performance of the CSN electrode was compared with that of an uncoated carbon electrode, as prepared in Example 1 (the control) as the cathode. The effective area of both electrodes was 10 cm². Although the CSN coating also serves as a cation exchange membrane (CEM), a CEM was still used in all experiments to ensure consistent charge efficiency so that the Ca^{2+} selective function of the CSN coating can be separated from its cation exchange function. A polypropylene mesh spacer with a 500 mm mesh opening and 61% porosity was installed between two ion exchange membranes to create a flow channel of ~1 mm in depth.

Characterization of Electrodes

After cryo-grinding and sonication in liquid nitrogen, the pulverized resin nanoparticles had an average particle diameter of 143±44 nm, 3 orders of magnitude smaller than its original size. SEM images showed that the prepared uncoated electrodes had a flat surface with a thickness of ~300 mm, and the activated carbon had a particle size of ~5 mm (FIGS. **21**A-**21**B).

Modification of the electrode with the CSN resulted in a dense, continuous coating of ~30 mm in thickness (FIGS. **21**C-**21**D) with resin nanoparticles well dispersed and distributed uniformly in the polymer matrix. FIG. **21**E compares FTIR spectra of the different electrodes as well as the unprocessed resin. The spectrum of the resin contained peaks of phosphonic (—PO_3) functional groups at 975 and 550 cm⁻¹, which offers high affinity to Ca^{2+} over Na^+. The CSN electrode clearly exhibited features of both the resin and the PVA/GA/SSA polymer matrix.

Evaluation of Electrode Performance

Similar to studies 1-3, performance parameters were employed to evaluate the overall capability of the prepared electrodes. In this study, such parameters included salt adsorption capacity (SAC, Formula 11), charge efficiency (Λ, Formula 12), and the amount of salt adsorbed at the end of the adsorption stage (q_T, Formula 13), wherein SAC measures the equilibrium adsorption capacity of the electrode, while Λ represents the percentage of the applied electric charges utilized for ion adsorption in the adsorption cycle.

$$SAC = q_T / S_{elec} \qquad\qquad \text{Formula 11}$$

$$\Lambda = F q_T \bigg/ \int_0^{t_{ad}} I(t)dt \qquad\qquad \text{Formula 12}$$

$$q_T = \int_0^{t_{ad}} Q \sum (C_{i,inf} - C_{i,eff})dt \qquad\qquad \text{Formula 13}$$

$$S_{t/c} = \frac{q_{T,t}}{q_{T,c}} \bigg/ \frac{C_{in,t}}{C_{in,c}} \qquad\qquad \text{Formula 14}$$

In the above Formulas, S_{elec} is the top surface area of two electrodes (m²); F is the Faraday constant (96,485 C/eq); t_{ad} is the duration of the adsorption stage in each adsorption/desorption cycle (1.5 h); 1(t) is electric current (A) at time t; Q is influent flow rate (L/s); and $C_{i,inf}$ and $C_{i,eff}$ are influent and effluent concentration (meq/L) of ion i. All reported values were average from at least three consecutive cycles.

It is noted that the salt adsorption capacity is based on the top surface area of the carbon electrode. Additionally, for the binary electrolyte solutions, a selectivity coefficient $S_{t/c}$ defined in accordance with the definition of ion exchanges processes (Formula 14) was employed to measure selectivity for the target (t) ion (Ca^{2+}) over the competeing ion (c) (Na^+).

In the single solute experiments the control (Example 1) and CSN electrodes (Example C5) were first evaluated separately in single solute experiments using feed solutions containing 10 meq/L NaCl or $CaCl_2$. A close examination of the conductivity profile revealed almost identical adsorption kinetics of the two electrodes for both NaCl and $CaCl_2$ (FIG. 22B). As demonstrated in FIG. 22A, highly reproducible current and conductivity profiles were observed in all cycles with both electrodes. During the desorption stage using reverse voltage, the control electrode exhibited a higher and sharper desorption peak than the CSN electrode (FIG. 22C). This suggests that the CSN coating slightly hindered ion transport back to the bulk solution, presumably due to the additional mass transfer resistance imposed by the CSN coating.

Despite the different valence and size of Ca^{2+} and Na^{2+}, their adsorption capacity by the uncoated electrode in terms of milliequivalent was similar 68.9 and 71.6 meq/m^2 for Ca^{2+} and Na^+, respectively in comparable initial concentrations (10 meq/L). As a comparison, the SAC of the CSN electrode was 77.3 and 78.0 meq/m^2 for Na^+ and Ca^{2+} respectively, 8% and 13% higher than the uncoated carbon electrode. The higher SAC may be attributed to increased charge efficiency (ratio of salt adsorption over charge in a CDI cycle), which was 78.7% ($CaCl_2$) and 86.9% (NaCl) for the uncoated electrode, and 86.4% (CaC_2) and 92.9% (NaCl) for the CSN electrode (FIG. 22D). This demonstrated improved performance of the modified CSN electrode of Example C5 relative to the control electrode of Example 1

In the binary solution experiments, solutions of NaCl and $CaCl_2$ with a total concentration of 10 meq/L and different Na^+-to-Ca^{2+} were used as the feed water to investigate Ca^{2+} adsorption in the presence of Nat The results are summarized in FIGS. 23A-C and 24.

The adsorption and desorption kinetic data (FIGS. 23A and 23B) revealed a substantial difference between the performance of the uncoated and CSN electrodes. The uncoated electrode exhibited notably faster Na^+ adsorption than Ca^{2+} adsorption despite the higher electrophoretic mobility of Ca^{2+}. This behavior may be attributed to the smaller radius of hydrated Na^+ (3.58 Å versus 4.12 Å for Ca^{2+}) and hence faster diffusion into the carbon pores, the rate limiting step of the electro-sorption process. About twice as much equivalents of Ca^{2+} (46.1±5.1 meq/m2) were adsorbed as Na^+ (24.7±2.5 meq/m2), resulting in a St/c of 1.9±0.1.

Unlike in the single salt $CaCl_2$ solution, the CSN coating greatly enhanced Ca^{2+} adsorption kinetics in the presence of Na^+ (FIG. 23A). It also increased the total SAC from 70.8±7.6 to 82.4±2.0 meq/m^2, a 16.4% increase, and although the SAC measured in mmol/m^2 remained unchanged (47.7±5.0 and 47.7±1.5 mmol/m2 for uncoated and CSN electrode, respectively, FIG. 23C). The improved equivalent salt adsorption by the CSN coating may be attributed to enhanced adsorption of Ca^{2+} relative to Na^+. As shown in FIG. 23C, Ca^{2+} adsorption (69.5±0.9 meq/m^2) by the CSN electrode was 50.7% higher than that of the uncoated electrode (46.1±5.1 meq/m^2), while Na^+ adsorp-

tion decreased by 48% (from 24.7±2.5 to 12.9±1.1 meq/m^2), resulting in a greatly improved Ca^{2+} selectivity ($S_{t/c}$) of 5.4.

CSN Selectivity Mechanism

As discussed above, the CSN coating increased Ca^{2+} adsorption relative to Na^+ on the carbon electrode, while having little direct contribution to Ca^{2+} adsorption capacity. In the previous Study 3, it was shown that selective SO_4^{2-} removal in the presence of Cl^- was achieved using a SO_4^{2-} selective coating on a carbon electrode which was due to preferential transport of SO_4^{2-} through the coating.

It is assumed that the same mechanism is responsible for the selective Ca^{2+} removal observed in the current study. To test this hypothesis, experiments were carried out in an electrodialysis cell to characterize ion transport through the CSN coating using a binary solution containing 5 meq/L of NaCl and 10 meq/L $CaCl_2$. By applying a constant current, the concentration of both Ca^{2+} and Na^+ decreased with operation time in the cation donor chamber, while a corresponding increase was observed in the ion acceptor chamber (FIG. 24).

Detailed mass balance analysis found that the decreased concentration of ions in the donor chamber was comparable with the accumulated ions in the accepting chamber with negligible ion adsorption on the CSN coated MF membrane, suggesting electro-migration of cations through the CSN MF under the electric field. The results further showed a 2.7 times higher Ca^{2+} migration flux (155.0 meq/m2-min) was achieved through the CSN coating than Na^+ (57.1 meq/m2-min) for a 2:1 (Ca^{2+}:Na^+) initial concentration ratio, despite the fact that Ca^{2+} had a larger hydrated ion size (4.12 Å for Ca^{2+} vs 3.58 Å for Na^+). The electro-migration flux of Ca^{2+} is ~2.7 times that of Na^+, which is comparable with the $S_{t/c}$ ratio between the CSN and uncoated electrodes (5.4/1.9) obtained in the electrosorption experiment at an influent Na^+-to-Ca^{2+} equivalent ratio of 1:1.

These results suggest that the higher affinity of the CSN electrode of Example C4 for Ca^{2+} resulted in the faster electro-migration rate of Ca^{2+} through the CSN coating, which is consistent with the solution diffusion model. The higher flux of Ca^{2+} relative to Na^+ would lead to a higher Ca^{2+}-to-Na^+ concentration ratio that the carbon electrode is exposed to, and therefore increased Ca^{2+} adsorption by the carbon electrode surface.

The CSN electrode was also shown to be reversible in long term operation, further demonstrating its long term performance.

In this study, a nanocomposite electrode (Example C4) was developed that selectively removes Ca^{2+} in the presence of competing Na^+ ions by applying a Ca^{2+}-selective nanocomposite (CSN) coating on the activated carbon electrode. The high affinity of the nanosized Ca^{2+} selective resin particles for Ca^{2+} ions results in higher Ca^{2+} permselectivity than Na^+, and hence an elevated Ca^{2+}-concentration in the carbon electrode pores, which leads to increased Ca^{2+} adsorption relative to the competing Na^+ The CSN electrode exhibited excellent performance over the long-term operation, with highly stable salt adsorption capacity, Ca^{2+} selectivity and regenerability.

Study 5 PEDOT:PSS Selective Coating

Desalination tests were conducted using porous electrodes only modified with a commercial CEM layer and porous electrodes prepared in accordance with Example C5 wherein the bound electrodes as prepared with electrodes of Examples 1 with ion-exchange coatings prepared from PEDOT:PSS solutions. Below, the performance of PEDOT:PSS MCDI (Example 5) and CEM only systems was first

compared, at varying applied voltages wherein the selectivity of the MCDI system for ions such as Na^+, Ca^{2+}, and Ba^{2+}.

Deionization tests were conducted in order to evaluate the selective ion removal performance of the prepared electrodes described above. A pair of ion selective polymer coated electrodes prepared in accordance with the Examples referenced above were inserted into a flow-by MCDI cell with a pair of ion exchange membranes and tested with the mixture of the monovalent and divalent ion feed solution. During operation, the CDI effluent was continuously measured in terms of conductivity and ion species. Mixed salt solutions containing two different concentrations (5 mM NaCl and 5 mM $CaCl_2$ (1:1)) were utilized in this study. The flow rate was 1 mL/min. The constant voltage was varied over the course of 7 different feed solutions experiments (#'s 1-7 in Table 2 below) and included 1.2 V and 6 V respectively. The adsorption/desorption cycle was 16.3 min.

The selectivity for specific ion adsorption was analyzed and calculated as described below in formulas 15-17.

$$\text{Fractional 'Na' removed} = \frac{Na_{feed} - Na_{eff}}{Na_{feed}} \qquad \text{Formula 15}$$

$$\text{Fractional 'Ca' removed} = \frac{Ca_{feed} - Ca_{eff}}{Ca_{feed}} \qquad \text{Formula 16}$$

$$\text{Selectivity (Ratio of fractional removal), } S_{Na}^{Ca} = \frac{Ca_{fr}}{Na_{fr}} \qquad \text{Formula 17}$$

The results of this study are summarized in Table 2 below.

TABLE 2

#	Feed solution	Voltage	Cation exchange layer	Na	Ca	Ba	Selectivity
1	10 mM, Na/Ca, 1:1	1.2	CEM only	0.27	0.34	NA	1.24
2	10 mM, Na/Ca, 1:1	1.2	CEM plus PEDOT PSS	0.28	0.39	NA	1.36
3	10 mM, Na/Ca, 1:1	0.6	CEM only	0.09	0.17	NA	2.01
4	10 mM, Na/Ca, 1:1	0.6	CEM plus PEDOT PSS	0.02	0.17	NA	6.98
5	10 mM, Na/Ba, 1:1	1.2	CEM plus PEDOT PSS	0.18	NA	0.39	2.21
6	10 mM, Na/Ba, 2:1	0.6	CEM plus PEDOT PSS	0.03	NA	0.19	6.23
7	13.3 mM, Na/Ca/Ba, 2:1:1	0.6	CEM plus PEDOT PSS	0.04	0.10	0.12	5.03

Provided in Table 2 and corresponding FIGS. 26-27, are the results from a comparison of the above prepared electrodes. The results of Experiment 1 and 2 are compared in FIG. 26A which clearly demonstrates a higher degree of selectivity is observed for the MCDI reactor comprising an electrode modified with a crosslinked PEDOT:PSS layer that was deposited on the porous electrode and positioned between the cation exchange membrane and the carbon electrode. A further comparison of Experiment 2 and 4 (FIG. 26B) shows that a decrease in the applied constant voltage from 1.2 V to 0.6 V results in a dramatic increase in selectivity towards Ca^{2+} over Na^+. FIG. 27A further demonstrates via comparison of Experiments 5 and 6 that a decrease in voltage shows an increase in selectivity towards Ba^{2+} over Ca^{2+}. Table 2 further shows that a cross-linked layer of PEDOT:PSS provides for an increased selectivity for Ba^{2+} over both Ca^{2+} and Na^+ when comparing Experiments 5-7 (FIG. 27B).

Although only a few example embodiments have been described in detail above, those skilled in the art will readily appreciate that many modifications are possible in the example embodiments without materially departing from this invention. Accordingly, all such modifications are

intended to be included within the scope of this disclosure as defined in the following claims.

What is claimed:

1. A method of forming an electrode for capacitive deionization, comprising:

depositing a slurry onto a substrate, wherein the slurry comprises a porous material, a first crosslinkable hydrophilic polymer, and a crosslinker for the first crosslinkable hydrophilic polymer;

annealing the slurry deposited on the substrate to create a crosslinked porous layer on the substrate;

depositing a solution comprising an ion-exchange material, a second crosslinkable hydrophilic polymer, and a crosslinker for the second crosslinkable hydrophilic polymer onto the crosslinked porous layer;

chemically modifying the crosslinked porous layer with iminodiacetic acid; and

optionally annealing and/or drying the solution on the crosslinked porous layer,

wherein the slurry and/or the solution are aqueous.

2. The method of claim 1, wherein depositing the slurry and/or solution is performed by one of spray coating, dip coating, spin coating, printing, slurry casting, or a flow-coating process.

3. The method of claim 1, wherein the porous material is selected from the group consisting of carbonaceous materials, metal organic framework, hexacyanoferrates, carbonized biomaterials and mixtures thereof.

4. The method of claim 1, wherein the first crosslinkable hydrophilic polymer is selected from the group consisting of polyvinyl alcohol, polyacrylic acid, polymethylmethacrylate, glycidylmethacrylate, partially sulfonated polystyrene polymers, polyamide, polyacrylamide, chitosan, or mixtures thereof.

5. The method of claim 4, wherein the crosslinker for the first crosslinkable hydrophilic polymer is at least one of sulfosuccinic acid, formaldehyde, glyoxal, adipic aldehyde, a dicarboxylic acid, a tricarboxylic acid, a polycarboxlic acid, anhydrides, acid chlorides, and glutaraldehyde.

6. The method of claim 1, wherein the ion-exchange material is an anion exchange polymer or a cation exchange polymer.

7. The method of claim 6, wherein the ion-exchange material is dispersed in particulate form into the solution prior to deposition of the solution onto the crosslinked porous layer.

8. The method of claim 1, wherein the second crosslinkable hydrophilic polymer is selected from the group consisting of polyvinyl alcohol, polyacrylic acid, polymethylmethacrylate, glycidylmethacrylate, partially sulfonated polystyrene polymers, polyamide, polyacrylamide, chitosan, or mixtures thereof.

9. The method of claim 8, wherein the crosslinker for the second crosslinkable hydrophilic polymer is at least one of

sulfosuccinic acid, formaldehyde, glyoxal, adipic aldehyde, a dicarboxylic acid, a tricarboxylic acid, a polycarboxlic acid, anhydrides, acid chlorides, and glutaraldehyde.

10. The method of claim **1**, wherein the slurry and the solution comprises no organic solvent.

11. A method of deionizing an aqueous fluid, comprising:

continuously flowing the aqueous fluid through a capacitive deionization reactor that includes at least one electrode fabricated according to claim **1** while applying a voltage between an anode and a cathode of the capacitive deionization reactor.

12. The method of claim **11**, further comprising:

regenerating the anode and the cathode by reversing the applied voltage.

13. A method of deionizing an aqueous fluid, comprising:

preparing at least one electrode by:

depositing a slurry onto a substrate, wherein the slurry comprises a porous material, a first crosslinkable hydrophilic polymer, and a crosslinker for the first crosslinkable hydrophilic polymer;

annealing the slurry deposited on the substrate to create a crosslinked porous layer on the substrate,

depositing a solution comprising an ion-exchange material, a second crosslinkable hydrophilic polymer, and a crosslinker for the second crosslinkable hydrophilic polymer onto the crosslinked porous layer;

chemically modifying the crosslinked porous layer with iminodiacetic acid; and

optionally annealing and/or drying the solution on the crosslinked porous layer,

wherein the slurry and/or the solution are aqueous; and

continuously flowing the aqueous fluid through a capacitive deionization reactor that includes the at least one electrode fabricated to selectively remove a targeted ion, while applying a voltage between an anode and a cathode of the capacitive deionization reactor.

14. The method of claim **13**, wherein the targeted ion selectively removed by the capacitive deionization reactor is at least one of monovalent cations, monovalent anions, multivalent cations and multivalent anions.

15. The method of claim **13**, wherein the capacitive deionization reactor is configured as a flow-by, flow-through, flow, faradaic, inverse, hybrid, or intercalating capacitive deionization reactor.

16. An apparatus for capacitive deionization reactions comprising:

a cathode;

an anode,

wherein at least one of the anode and/or cathode is a crosslinked porous electrode formed by the method of claim **1**,

wherein the crosslinked porous electrode comprises substrate, a first porous layer deposited on the substrate, and a second layer deposited on the first porous layer;

wherein the first porous layer comprises a porous material and a crosslinked hydrophilic polymer, and the second layer comprises an ion exchange material, a crosslinked or non-crosslinked hydrophilic polymer, and optionally a crosslinker.

17. The apparatus of claim **16**, wherein the crosslinked ion-exchange layer is selective for at least one of monovalent cations, monovalent anions, multivalent cations and multivalent anions.

* * * * *